

Copyright © 1994, by the author(s).
All rights reserved.

Permission to make digital or hard copies of all or part of this work for personal or classroom use is granted without fee provided that copies are not made or distributed for profit or commercial advantage and that copies bear this notice and the full citation on the first page. To copy otherwise, to republish, to post on servers or to redistribute to lists, requires prior specific permission.

**MULTI-CARRIER CDMA IN AN INDOOR
WIRELESS RADIO CHANNEL**

by

Nathan Yee and Jean-Paul Linnartz

Memorandum No. UCB/ERL M94/6

5 February 1994

MICRO Project (93-101)

**MULTI-CARRIER CDMA IN AN INDOOR
WIRELESS RADIO CHANNEL**

by

Nathan Yee and Jean-Paul Linnartz

Memorandum No. UCB/ERL M94/6

5 February 1994

MICRO Project (93-101)

ELECTRONICS RESEARCH LABORATORY

College of Engineering
University of California, Berkeley
94720

**MULTI-CARRIER CDMA IN AN INDOOR
WIRELESS RADIO CHANNEL**

by

Nathan Yee and Jean-Paul Linnartz

Memorandum No. UCB/ERL M94/6

5 February 1994

MICRO Project (93-101)

ELECTRONICS RESEARCH LABORATORY

College of Engineering
University of California, Berkeley
94720

This report summarizes the research findings of the MICRO project 93-101, entitled "Frequency - Code Division Multiple Access: a New Spreading Technique for Radio Communications over Multipath Channels", supported by Teknekron Communication Systems, Berkeley and the California MICRO Program. Principal Investigator is Professor J.P. Linnartz, Industrial Liaison is Dr. G. Fettweis.

Table of Contents

CHAPTER 1	<i>Introduction</i>	1
	1.1 Introduction	1
CHAPTER 2	<i>Multipath Channels</i>	3
	2.1 Multipath Channels	3
CHAPTER 3	<i>Principles of MC-CDMA</i>	6
	3.1 What is MC-CDMA?	6
	3.2 The F-parameter	7
	3.3 Comparison with Conventional Modulation Techniques	8
	3.4 The Indoor Environment and MC-CDMA	10
	3.5 The Codes	11
	3.6 Transmitter Model	11
	3.7 Channel Model	13
	3.8 Receiver Model	14
	3.9 Equalization	16
CHAPTER 4	<i>Analysis of the Performance of MC-CDMA in Rayleigh and Rician Fading Channels</i>	20
	4.1 Rayleigh Fading	20
	4.2 Rician Fading	28
CHAPTER 5	<i>Numerical Results</i>	33
	5.1 Rayleigh Fading	33
	5.2 Rician Fading	38
CHAPTER 6	<i>Conclusion</i>	44
Appendix A	<i>Statistical Properties of the Noise</i>	46
Appendix B	<i>Statistical Properties of the Interference</i>	49
Appendix C	<i>Simplification of CLT Expressions</i>	52
	<i>References</i>	53

1.1 Introduction

With a surging increase in demand for personal wireless radio communications within the past decade, there is a growing need for technological innovations to satisfy these demands. Future technology must be able to allow users to efficiently share common resources, whether it involves the frequency spectrum, computing facilities, databases, or storage facilities. As with mobile cellular telephony, the driving forces behind this demand includes the mobility and flexibility that this technology provides. In contrast to wired communications, future personal communication networks will allow users the connection to a multitude of resources while enjoying the freedom of mobility. A particular area of growing interest is indoor wireless communications.

In an indoor environment, the use of a wireless communication link removes any need for wiring. Besides the removal of the costs associated with wiring, wireless links allow the network to operate undisturbed while new users are added.

While there is a strong desire for this technology, there are many obstacles and issues that need to be addressed. The issue of portability places constraints on the size and on the power consumption of the terminals. In addition, transmissions in an indoor environment face the harsh degradations of multipath channels.

In this document, a novel digital modulation and multiple access scheme called Multi-Carrier CDMA (MC-CDMA) [1] [2] [3] is analyzed. Although this modulation technique in this report is applied primarily to an indoor wire-

less radio network, this transmission scheme may have other applications. One possible application is vehicle-to-vehicle communications for Intelligent Highway Vehicle Systems (IHVS). The deciding factors on whether this technique is feasible for a certain application depends largely on the physical channel and the baud rates of interest. Under appropriate conditions, MC-CDMA signals will propagate through multipath channels with little distortion¹.

Although MC-CDMA resembles the signal structure for OFDM when the subcarriers are spaced as closely as possible, the manner in which the subcarriers are utilized is very different. In [4] [5], OFDM is discussed as a means of decreasing the effective baud rate by transmitting different data symbols on different subcarriers. With MC-CDMA, the same data bit is transmitted over all subcarriers without changing the original baud rate.

In [3], a bound on the bit error rate for convolutionally-coded MC-CDMA is presented. In this scheme, a maximum-likelihood detection is performed on the received signal where all signals including the interference are considered in the decision making process. For the MC-CDMA system that we are analyzing, the receiver is assumed to be of a much simpler form, detecting only for the desired signal using classical diversity theory.

The general organization of this document is as follows. The discussion begins with the review of multipath channels and its implications on wireless communications. In Chapter 3, MC-CDMA is described in detail. It is compared to other conventional modulation techniques; differences and similarities are pointed out. In the process, motivations for this new technique are discussed. Next, implementation of this modulation scheme will be discussed with a possible transmitter and receiver model. In the receiver model, different frequency equalization techniques are considered. In Chapter 4, the performance of this technique in an indoor wireless environment is evaluated for Rayleigh and Rician fading channels. Numerical results are presented and discussed in Chapter 5.

1. In this report, "distortion" means linear distortion or dispersion.

CHAPTER 2 *Multipath Channels*

2.1 Multipath Channels

When a binary phase-shift keying (BPSK) modulated signal is transmitted over a wireless channel, the transmitted signal decomposes into multiple copies of the original signal corresponding to multiple path reflections off of the surrounding environment. Each path will experience an attenuation, a phase delay and a time delay. At the receiver, the received signal consists of the superposition of these paths. Because of the random nature of the channel effects mentioned above, the paths may add destructively. This phenomenon creates an obstacle for wireless communications.

Two parameters that are often used to characterize multipath channels are the delay spread and the coherence bandwidth [6]. The delay spread, T_d , is a measure of the length of the impulse response of the channel. Delay spreads lead to intersymbol interference (ISI) and consequently degrade the performance of the system and complicate the receiver design. In indoor environments, the root mean square (r.m.s) delay spread is in general small with typical values in the range of 10 - 50 ns. [7]. Also of interest is the number of resolvable paths, which is defined to be

$$L = \left\lfloor \frac{T_m}{T_b} \right\rfloor + 1 \quad (1)$$

where T_d is the maximum delay spread and T_b is the symbol duration. For narrowband communications, there is usually only one resolvable path for transmission rates up to 1 Mbauds/sec.

As a measure of the correlation of the fading between frequencies, the coherence bandwidth is directly related to the delay spread. For an exponentially distributed delay spread power profile, the coherence bandwidth is given as

$$BW_c = \frac{1}{2\pi T_d}. \quad (2)$$

Two frequencies lying within the coherence bandwidth are likely to experience correlated fading.

Another channel phenomenon associated with wireless communications is the Doppler spread. While it may be interpreted as a measure of the variation of the shift in the carrier frequency, it is in some ways more intuitive to view it as a measure of the rate at which the channel changes. Small doppler spreads imply a large coherence time or a slowly changing channel. Measurements indicate that Doppler shifts are relatively small and typically in the range of 0.3 to 6.1 Hz [8] in the indoor environment. Thus, the channel may be assumed to be constant over the symbol duration, T_b , for baud rates up to 1 Mbaud/sec.

Within a small time window in which the effects of the channel are relatively constant, the received signal consists of the contribution from the paths that arrive within this interval. Each path may be treated as a vector with an amplitude and phase. If the terminal is moving or the surrounding environment is changing, the effects of the channel will randomly change with time. Thus, at some points in time, the paths may add destructively and in others constructively. Obviously, the case that is undesirable is when the channel attenuates the signal. Two distributions that are commonly used to describe the random amplitudes resulting from multipath channels are the Rayleigh and Rician distributions.

If there is no line-of-sight (LOS) component in the received signal, i.e., when the direct path is obstructed as with propagation in an outdoor environment over long distances, the received signal consists only of scattered components due to reflections with no dominant path. The received signal can be separated into an in-phase and a quadrature component where each path will contribute an in-phase and a quadrature component. Assuming that there are a very large number of paths, the in-phase and quadrature components can be assumed to be zero-mean Gaussian random variables by the Central Limit Theorem (CLT). Thus, the overall amplitude of the signal that results from the vector addition of all components is by definition Rayleigh distributed and the phase is uniformly distributed on the interval of $[0, 2\pi]$.

The Rayleigh distribution of ρ is defined to be

$$f_{\rho}(\rho) = \frac{\rho}{\sigma^2} e^{-\left(\frac{\rho^2}{2\sigma^2}\right)} \quad (3)$$

where σ^2 is the variance of the in-phase and quadrature components. Two statistical quantities of interest are the mean and the second moment of the Rayleigh random variable. They can be determined to be

$$E\rho = \sqrt{\frac{\pi}{2}}\sigma \quad E\rho^2 = 2\sigma^2. \quad (4)$$

If there is a direct LOS component, as in the case of indoor environments, the received signal will most likely consist of a dominant component corresponding to the LOS path and a scattered component due to reflections. Arbitrarily

orienting the in-phase and quadrature components so that the LOS component is in-phase, the received signal amplitude, ρ , has a Rician distribution given by

$$f_{\rho}(\rho) = \frac{\rho}{\sigma^2} e^{-\frac{\rho^2 + b_0^2}{2\sigma^2}} I_0\left(\frac{b_0\rho}{\sigma^2}\right) \quad (5)$$

where σ^2 represents the power of the scattered in-phase and quadrature components, b_0 is the amplitude of the LOS component and $I_0(\rho)$ is the zeroth order modified Bessel function. The Rician distribution is often characterized by the Rician K -factor, which is defined to be the ratio of the power of the LOS component to the power of the scattered component and is given as

$$K = \frac{b_0^2}{2\sigma^2}. \quad (6)$$

Measurements of the indoor environments indicate that a Rician K -factor of 10 is a typical value for an open-office interior floor plan [9] [10]. A statistical quantity that is of interest is the mean of the Rician distribution which can be found to be

$$E\rho = e^{-K/2} \sqrt{\frac{\pi}{2(K+1)}} \bar{P} \left[(1+K) I_0\left(\frac{K}{2}\right) + K I_1\left(\frac{K}{2}\right) \right] \quad (7)$$

where $I_1(K)$ represents the first order modified Bessel function.

Many studies have been done on the channel modelling of indoor environments. The statistical models given in [11] [12] may be more appropriate for wideband signals where there are many resolvable paths rather than in narrow-band communications where there is usually one resolvable path (i.e., $T_d \ll T_b$).

CHAPTER 3 *Principles of MC-CDMA*

3.1 What is MC-CDMA?

Multi-carrier CDMA is a digital modulation technique where a single data symbol is transmitted at multiple narrow-band subcarriers with each subcarrier encoded with a phase offset of 0 or π based on a spreading code. The narrowband subcarriers are generated using BPSK modulated signals, each at different frequencies which at baseband are at multiples of a harmonic frequency, $1/T_b$. Consequently, the subcarriers are orthogonal to each other at baseband, and the component at each subcarrier may be filtered out by modulating the received signal with the frequency corresponding to the particular subcarrier of interest and integrating over a symbol duration. The orthogonality between subcarrier frequencies is maintained if the subcarrier frequencies are spaced apart by multiples of F/T_b where F is an integer. Throughout this document, F , which will be used to describe the spacing between subcarrier frequencies for an MC-CDMA signal, will be referred to as the F -parameter. An example of an MC-CDMA signal in the frequency domain for $F = 6$ is shown in Fig. 1c.

The phase at each subcarrier corresponds to one element of the spreading code. For a spreading code of length N , there are N subcarriers. Throughout this paper, N will be referred to as the spreading factor. This modulation scheme is also a multiple access technique in the sense that different users will use the same set of subcarriers but with a different spreading code that is orthogonal to the code of all other users. Thus, it is important to point out that there exist two levels of orthogonality. While the subcarriers frequencies are orthogonal to each other, and the spreading codes are also orthogonal to each other.

Upon careful examination, the discrete-time version of the signal can be viewed as the Discrete Fourier Transform (DFT) of a Direct Sequence - Code Division Multiple Access (DS-SS-CDMA) signal, i.e., the signal is CDMA-coded in fre-

quency. This scheme can also be considered as a spread spectrum technique since the signal is spread over a larger bandwidth than necessary in order to achieve frequency diversity.

3.2 The F-parameter

In order to obtain a compact signal in frequency, it would be desirable to space the subcarriers as closely together as possible. The closest possible spacing between subcarriers is $1/T_b$, where $F = 1$. With this particular spacing, the structure of the signal is exactly that of Orthogonal Frequency Division Multiplexing (OFDM) [4] [5].

3.2.1 $F = 1$ and OFDM

Although OFDM and MC-CDMA have the same signal structure, they are very different in how the subcarriers are actually used to transmit data. With OFDM, different data symbols are transmitted at different subcarriers. These sets of data symbols can be encoded with error correction or detection codes to compensate for the loss of individual subcarriers and their corresponding data symbols. The goal of OFDM is to reduce the effective transmission rate and consequently increase the symbol duration. As a result, the OFDM signal is affected less by delay spreads and ISI because of the longer symbol duration. In addition, if the channel changes rapidly, i.e., when there are large Doppler shifts, the longer symbol duration helps to average out the signal over these fluctuations and occurrences of deep fades in time. The implementation of multiple access in OFDM is different from that of MC-CDMA in that different users do not use the same set of subcarriers. Multiple access in OFDM may be implemented by having different users transmit on different sets of subcarriers (frequency division multiplexing) or to have different users contribute to a data set that will be assigned to the same OFDM signal. Thus, as it can be seen, OFDM and MC-CDMA differ greatly in the utilization of the subcarriers.

Since MC-CDMA has the same signal structure for $F = 1$ as OFDM, some conclusions and results about OFDM can be applied to MC-CDMA for $F = 1$. One conclusion is that MC-CDMA for $F = 1$ is spectrally efficient. Since the subcarriers are spaced closely together, an efficient bits/Hz ratio is obtained [5]. In addition, since the edges of the signal in frequency are formed by narrowband *sinc*() functions, the drop off of the MC-CDMA ($F = 1$) signal spectrum at its edges is very sharp. Consequently, the spectral leakage into adjacent frequency bands is small. Another conclusion that can be drawn from the similarity with OFDM will be brought up when the implementation aspects of MC-CDMA are discussed.

3.2.2 F very Large

While one would desire a spectrally compact and efficient signal, there is also the conflicting goal of frequency diversity. By transmitting the signal at multiple subcarriers, it is hoped that only a few of the subcarriers will be severely attenuated with the majority of the subcarriers passing through the channel with little distortion. The degree to which this goal coincides with the physical channel depends on the coherence bandwidth, BW_c , of the channel. If several subcarriers lie within the coherence bandwidth, then it is statistically likely that the loss of one subcarrier implies the loss of all the subcarriers within BW_c . In this case, frequency diversity is not achieved.

Consequently, depending on the actual physical channel, one may desire to space the subcarriers as far apart as possible, corresponding to a large F -parameter, in order to obtain frequency diversity. This implies that frequency diversity can be achieved with a relatively small spreading factor with MC-CDMA using an appropriate value for F . While this may not make the MC-CDMA signal spectrally compact, a possible solution is to have other programs or applications (not necessarily constructed of MC-CDMA signals) assigned to the gaps between the narrowband subcarriers.

3.3 Comparison with Conventional Modulation Techniques

In order to understand the motivations for MC-CDMA, it is helpful to compare it with other conventional modulation techniques.

3.3.1 Narrowband (BPSK) signals

Narrowband communications [13] has the desirable quality of being relatively immune to intersymbol interference in an indoor environment as the symbol duration is greater than the delay spread ($T_d \ll T_b$). However, this same condition implies that the signal bandwidth is smaller than the coherence bandwidth. Consequently, a narrowband signal will experience the undesirable effect of experiencing flat fading. Depending on the location of the receiver, the entire signal may be located in a deep fade that significantly attenuates the entire signal (see Fig. 1a).

3.3.2 Direct Sequence - Spread Spectrum Code Division Multiple Access

To combat the effect of flat fading, conventional DS-SS Spread Spectrum [14] [15] may be applied so that the signal bandwidth is spread over a bandwidth larger than the coherence bandwidth. A DS-SS signal is generated by mul-

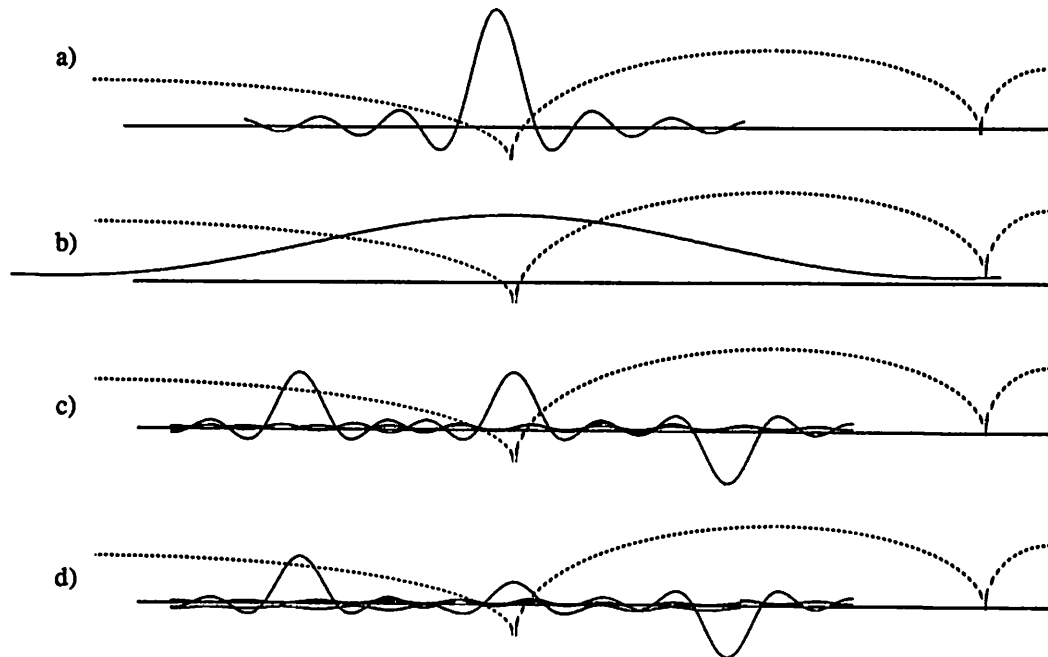


Fig. 1 Spectrum of a) Narrowband signal, b) DS-CDMA signal, c) MC-CDMA signal before the channel, and d) MC-CDMA after the channel. The (---) represents the channel while the solid line represents the signal.

tipling each user data symbol by a fast binary antipodal sequence where the chip duration is T_b/N . These faster variations in time increase the bandwidth of the signal. Consequently, if the spreading factor is sufficiently large, the signal experiences frequency-selective fading, and it is unlikely that the entire signal will be lost to fades in frequency (see Fig 1b).

In the process of generating this signal, the resolution in time at the receiver is increased by a factor of N , and the signal is more susceptible to inter-chip interference. This inter-chip interference results in complexity in the design of the receiver and synchronization issues that must address the increase in the number of resolvable paths. One method of implementing the receiver is with a Rake receiver where the receiver consists of multiple branches of receivers, each synchronized in time to a resolvable path. If T_b/N is very small compared to T_d , then the number of branches (resolvable paths) in the Rake receiver will be prohibitively large.

Although the implementation of the Rake receiver is possible, there are complications and limitations that arise for certain applications. With indoor wireless office communications, there is the issue of power consumption. The portable terminals are designed under a low power consumption constraint. Measurements of the indoor wireless radio channel

have shown that some bands of frequency, such as the deregulated ISM band, have a relatively flat channel and a large coherence bandwidth. In order to achieve frequency diversity with a DS-CDMA system in such an environment, very large spreading factors would be required. This large spreading factor translates to a prohibitively large power consumption due to signal processing and synchronization. In addition, large spreading factors would imply the usage of a large physical bandwidth and consequently a spectrally inefficient allocation of resources.

3.3.3 MC-CDMA

MC-CDMA addresses the issue of how to spread the signal bandwidth without increasing the adverse effect of the delay spread. As a MC-CDMA signal is composed of N narrowband subcarrier signals each of which has a symbol duration much larger than the delay spread, a MC-CDMA signal will not experience an increase in susceptibility to delay spreads and ISI as does DS-CDMA. In addition, since the F -parameter can be chosen to determine the spacing between subcarrier frequencies, a smaller spreading factor than one required by DS-CDMA can be used to make it unlikely that all of the subcarriers are located in a deep fade in frequency and consequently achieve frequency diversity (see Fig. 1c and d).

3.4 The Indoor Environment and MC-CDMA

In an indoor environment, the characteristics of the channel allow for an MC-CDMA signal to experience relatively little distortion. As mentioned in the section on multipath channels, indoor wireless radio channels are typically characterized by small delay spreads and small doppler shifts. As mentioned above, MC-CDMA signals are composed of narrowband subcarrier signals with a symbol duration greater than the delay spread. Equivalently, the signal bandwidth is smaller than the coherence bandwidth. Thus, the channel that each subcarrier experiences can be approximated as flat fading which only attenuates the entire signal leaving the general shape of the signal undistorted. Thus, this reasoning implies that the lengthening or dispersion of the signal in time is negligible. Small doppler shifts are desirable for MC-CDMA signals since doppler shifts larger than or on the order of the bandwidth of the narrowband signals would make the reception of these signals very difficult.

3.5 The Codes

Up until now, we have been very vague about the specific spreading codes that may be used. In this section, we will discuss possible codes that may be used. The length of the codes are assumed to be equal to the number of subcarriers, N . The individual elements of the code will be referred to as chips. Each chip of a code belongs to the set $\{1, -1\}$. The property of the codes that is desired is for the codes of different users to be orthogonal, i.e.,

$$\sum_{i=0}^{N-1} c_l[i] c_m[i] = N\delta_{l,m}. \quad (8)$$

One possible set of codes are the pseudo-random codes (pn-codes) generated by shift registers. These codes are called pseudo-random because they appear to be random with a balanced run of -1's and 1's. Using a shift register of length n , the length of the code that is generated is $2^n - 1$. Thus, only odd length codes can be generated. This observation implies that the codes are not perfectly orthogonal since there is not a perfect balance between -1's and 1's. To be precise, the inner product between any two different pn-codes is -1. In addition, if the transmitter is to be implemented with an FFT, the code length should be a multiple of 2, which is not possible with pn-codes.

Another possible set of codes are the Walsh-Hadamard codes. These codes are generated by matrix operations. The basic matrix unit of Walsh-Hadamard code generation is

$$H_0 = \begin{bmatrix} 1 & 1 \\ 1 & -1 \end{bmatrix}. \quad (9)$$

Walsh codes of length 2^n can be generated with the following recursive matrix operation

$$H_n = \begin{bmatrix} H_{n-1} & H_{n-1} \\ H_{n-1} & -H_{n-1} \end{bmatrix} \quad (10)$$

where the matrix, H_n , of size $2^n \times 2^n$ is formed using the matrix, H_{n-1} , of size $2^{n-1} \times 2^{n-1}$ with H_0 given in Eq. (9). Each row of the matrix, H_n , gives the code for one user. It can be verified that these codes are perfectly orthogonal in the sense that the inner product between any two different codes (rows of the matrix) is zero.

3.6 Transmitter model

Shown in Fig. 2 is a model of the transmitter for one possible implementation of an MC-CDMA system. The input data symbols, $a_m[k]$, are assumed to be binary antipodal where k denotes the k th bit interval and m denotes the m th user. In the analysis, it is assumed that $a_m[k]$ takes on values of -1 and 1 with equal probability. The generation of an MC-CDMA

signal can be described as follows. A single data symbol is replicated into N parallel copies. The i th branch (subcarrier) of the parallel stream is multiplied by a chip, $c_m[i]$, from a pseudo-random (PN) code or some other orthogonal code of length N and then BPSK modulated to a subcarrier spaced apart from its neighboring subcarriers by F/T_b , where F is an integer number. The transmitted signal consists of the sum of the outputs of these branches. This process yields a multi-carrier signal with the subcarriers containing the PN-coded data symbol.

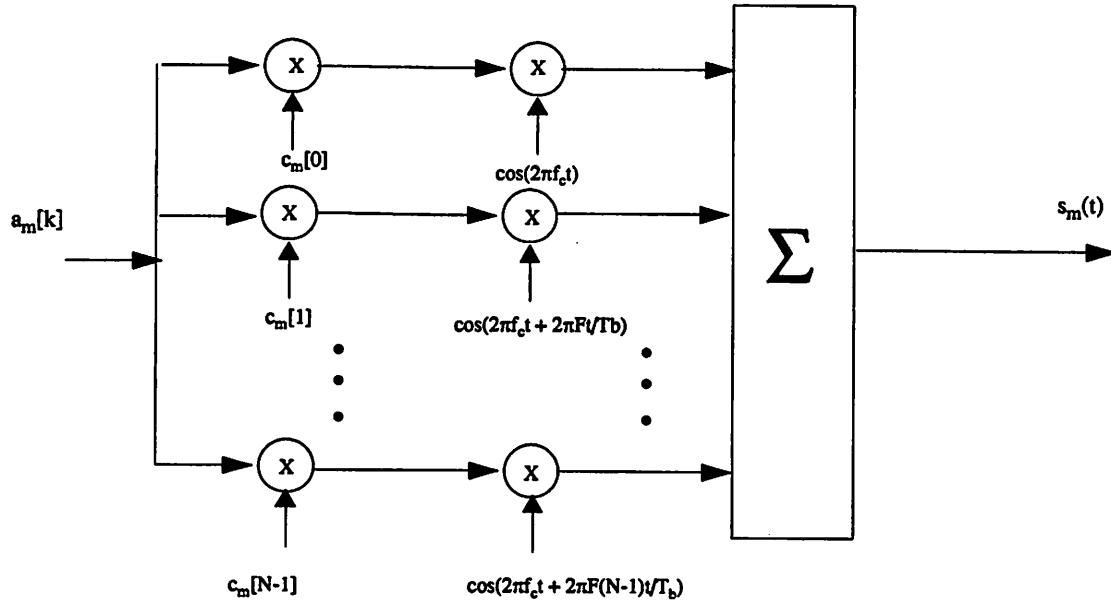


Fig. 2 Transmitter Model

Observing the model of the transmitter in Fig. 2, the implementation of an MC-CDMA transmitter appears prohibitive with the bank of oscillators, one for each of the subcarriers. However, it should be noted for the case of $F = 1$, as mentioned above, the MC-CDMA signal shares the same signal structure as OFDM. The analysis of OFDM has shown that the discrete-time version of the OFDM transmitter is simply a Discrete Fourier Transform (DFT). Thus, the transmitter model of MC-CDMA in Fig.2 may simply be replaced by an FFT operation for $F = 1$. In the analysis, we will assume a continuous-time receiver model as shown in Fig. 2. This model makes the analysis simpler and more instructive.

As illustrated in Fig. 2, the transmitted signal corresponding to the k th data bit of the m th user is

$$s_m(t) = \sum_{i=0}^{N-1} c_m[i] a_m[k] \cos(2\pi f_c t + 2\pi i \frac{F}{T_b} t) p_{T_b}(t - kT_b) \quad (11)$$

$$c_m[i] \in \{-1, 1\}$$

where $c_m[0], c_m[1], \dots, c_m[N-1]$ represents the spreading code of the m th user and $p_{T_b}(t)$ is defined to be a unit amplitude pulse that is non-zero in the interval of $[0, T_b]$.

3.7 Channel Model

In Chapter 2, multipath channels were discussed and the common distribution functions encountered when characterizing the random amplitude effects of the channel were described. A more detailed discussion of the channel model that is appropriate for MC-CDMA systems in an indoor environment will follow.

In this document, we will focus on a frequency-selective channel with $1/T_b \ll BW_c \ll F/T_b$. For the symbol rates of interest, this model implies that each modulated subcarrier with transmission bandwidth of $1/T_b$ does not experience significant dispersion ($T_b \gg T_d$) and overlapping between adjacent data symbols (ISI). It is also assumed that the amplitude and phase remain constant over a symbol duration, T_b , (i.e., Doppler shifts due to the motion of terminals and the surrounding environment are negligible) which as mentioned earlier is a reasonable assumption. The condition $BW_c \ll F/T_b$ implies that for different subcarriers the fading is assumed to be independent. For symbol rates on the order of 1 Mbauds/sec, this assumption is reasonable since the symbol duration of 1×10^{-6} secs is much larger than the typical r.m.s delay spreads of 50 ns.

Assuming flat fading at the subcarriers, the effects of the channel for a signal subcarrier can be characterized by 2 parameters: an amplitude scaling and a phase distortion. The transfer function of the continuous-time fading channel assumed for the m th user in the indoor environment can be represented as

$$H_m \left[f_c + i \frac{F}{T_b} \right] = \rho_{m,i} e^{j\theta_{m,i}} \quad (12)$$

where $\rho_{m,i}$ and $\theta_{m,i}$ are the random amplitude and phase effects of the channel of the m th user at frequency $f_c + i(F/T_b)$. In addition, as mentioned above, it is assumed that the $\rho_{m,i}$ and $\theta_{m,i}$ remain approximately constant over the symbol duration, T_b .

The local-mean power at the i th modulated subcarrier of the m th user is defined to be

$$\overline{P_{m,i}} = E \left[\rho_{m,i} \cos \left(2\pi f_c t + 2\pi i \frac{F}{T_b} t + \theta_{m,i} \right) \right]^2 = \frac{1}{2} E \rho_{m,i}^2 \quad (13)$$

where the iid assumptions imply that the local-mean powers, $\overline{p_{m,i}}$, of all subcarriers are equal. Thus, the total local-mean power of the m th user is defined to be $\overline{p_m} = N\overline{p_{m,i}}$.

An important distinction to make in the channel model is the difference between uplink and downlink transmissions. Transmissions in these different directions lead to very different effects on the transmitted signal.

3.7.1 Uplink

With uplink transmissions, i.e., transmissions from the terminals to the base station, the base station receives the signals from different terminals through different channels. Thus, there is a set of random amplitudes, $\{\rho_{m,i}\}_{i=0}^{N-1}$, and a set of random phases, $\{\theta_{m,i}\}_{i=0}^{N-1}$, associated with each user for $m = 0, 1, \dots, M-1$. In the analysis, it is assumed that these random variables are independent between users. This assumption implies that any amplitude or phase correction performed on the desired signal of the received signal does not simultaneously correct for the amplitude and phase of the interference.

3.7.2 Downlink

For transmissions in the downlink, i.e., transmissions from the base station to the terminals, a terminal receives interfering signals designated for other users ($m = 1, 2, \dots, M-1$) through the same channel as the wanted signal ($m = 0$). Thus, there is only one set of amplitudes and phases describing the channel for all user signals. This observation can be included in the notation by repressing the user index in the channel variables for downlink transmissions

$$\rho_{m,i} = \rho_{0,i} \quad \theta_{m,i} = \theta_{0,i} \quad \forall m. \quad (14)$$

This observation implies that when amplitude or phase correction is applied on the wanted signal, the amplitude and phase of the interfering signals will also be corrected.

3.8 Receiver Model

When there are M active users, the received signal is

$$r(t) = \sum_{m=0}^{M-1} \sum_{i=0}^{N-1} \rho_{m,i} c_m[i] a_m[k] \cos(2\pi f_c t + 2\pi i \frac{F}{T_b} t + \theta_{m,i}) + n(t) \quad (15)$$

where the effects of the channel have been included in $\rho_{m,i}$ and $\theta_{m,i}$ and $n(t)$ is additive white Gaussian noise (AGWN) with a one-sided power spectral density of N_0 . Assuming the transmitter model of Fig. 2, a possible implementation of

the receiver is shown in Fig. 3 where it has been assumed that $m = 0$ corresponds to the desired signal. With this model, there are N matched filters with one matched filter for each subcarrier. The output of each filter contributes one component to the decision variable, v_o . Each matched filter consists of an oscillator with a frequency corresponding to the frequency of the particular BPSK modulated subcarrier that is of interest and an integrator. In addition, a phase offset equal to the phase distortion introduced by the channel, $\theta_{0,i}$, is included in the oscillator to synchronize the receiver to the desired signal in time. To extract the desired signal's component, the orthogonality of the codes is used. For the i th subcarrier of the desired signal, the corresponding chip, $c_0[i]$, from the desired user's code is multiplied with it to undo the code. If the signal is undistorted by the channel, the interference terms will cancel out in the decision variable due to the

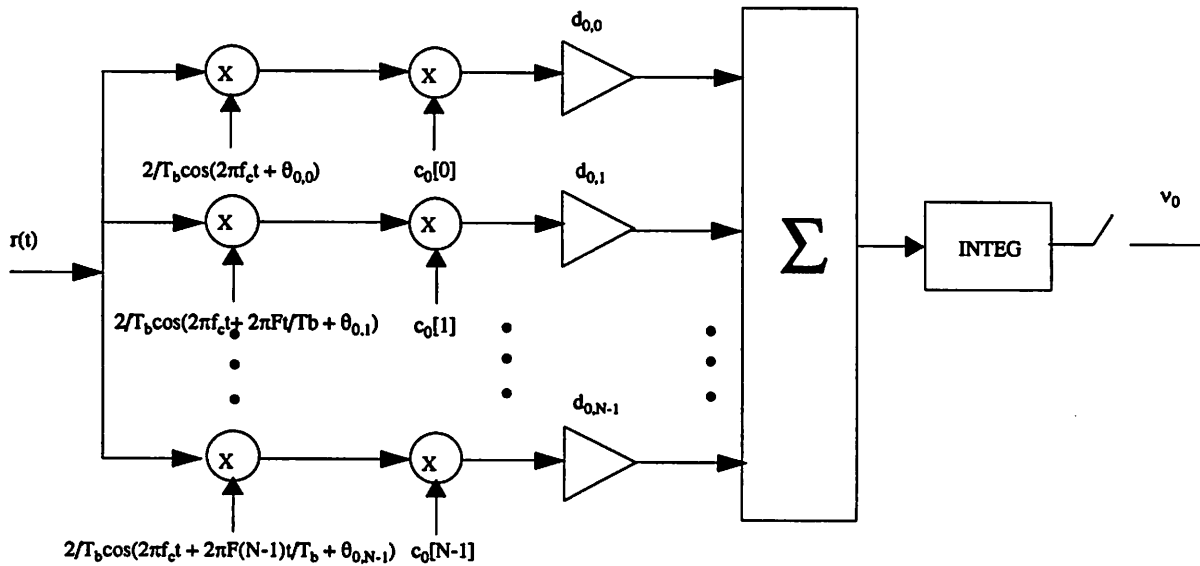


Fig. 3 Receiver Model

orthogonality of the codes. This comment will be discussed in detail in the next paragraph. As the channel will distort the subcarrier components, an equalization gain, $d_{0,i}$, may be included for each matched filter branch of the receiver.

Applying the receiver model of Fig. 3 to the received signal given in Eq. (15) yields the following decision variable for the k th data symbol assuming the users are synchronized in time

$$v_o = \sum_{m=0}^{M-1} \sum_{i=0}^{N-1} \rho_{m,i} c_m[i] d_{0,i} a_m[k] \frac{2}{T_b} \int_{kT_b}^{(k+1)T_b} \cos(2\pi f_c t + 2\pi i \frac{F}{T_b} t + \theta_{m,i}) \cos(2\pi f_c t + 2\pi i \frac{F}{T_b} t + \hat{\theta}_{0,i}) dt + \eta \quad (16)$$

where $\hat{\theta}_{0,i}$ denotes the receiver's estimation of the phase at the i th subcarrier of the desired signal and the corresponding AWGN term, η , is given as

$$\eta = \sum_{i=0}^{N-1} \int_{kT_b}^{(k+1)T_b} n(t) \frac{2}{T_b} d_{0,i} \cos(2\pi f_c t + 2\pi i \frac{F}{T_b} t + \hat{\theta}_{0,i}) dt. \quad (17)$$

Assuming perfect phase correction, i.e., $\hat{\theta}_{0,i} = \theta_{0,i}$, the decision variable reduces to

$$v_o = a_0[k] \sum_{i=0}^{N-1} \rho_{0,i} d_{0,i} + \sum_{m=1}^{M-1} \sum_{i=0}^{N-1} a_m[k] c_m[i] c_0[i] \rho_{m,i} d_{0,i} \cos \bar{\theta}_{m,i} + \eta \quad (18)$$

where $\bar{\theta}_{m,i} = \theta_{0,i} - \theta_{m,i}$. Note that if $\theta_{0,i}$ and $\theta_{m,i}$ are iid uniform r.v.'s on the interval $[0, 2\pi]$, then $\bar{\theta}_{m,i}$ is also uniformly distributed on the interval $[0, 2\pi]$. Note that the decision variable consists of three terms. The first term corresponds to the desired signal's component, the second corresponds to the interference and the last corresponds to a noise term.

To illustrate the desired effect of the codes, consider the case of a perfect channel where $\rho_{m,i} = 1$ and $\theta_{m,i} = 0$. In a perfect channel, the decision variable is given as

$$v_o = N a_0[k] + \sum_{m=1}^{M-1} a_m[k] \sum_{i=0}^{N-1} c_m[i] c_0[i] + \eta \quad (19)$$

where all interference terms cancel out because of the orthogonality of the codes. Unfortunately, in real multipath channels, this is unlikely to happen and each subcarrier will experience fading. This leads to the question of what form of equalization should be performed.

3.9 Equalization

The question of what equalization technique should be used must address different issues. The underlying goal of these techniques should be to reduce the effect of the fading and the interference while not enhancing the effect of the noise on the decision of what data symbol was transmitted. Whenever there is a diversity scheme involved whether it may involve receiving multiple copies of a signal from time, frequency or antenna diversity, the field of classical diversity theory can be applied. These equalization techniques may be desirable for their simplicity as they involve simple multiplications with each copy of the signal. However, they may not be optimal in a channel with interference in the sense of minimizing the error under some criterion. In some ways, these equalization scheme appear "ad hoc" as they are not derived under some clear procedure.

It should be noted that while there are some decision making techniques, such as Viterbi decoding and Wiener filtering, that are optimal in the sense that they minimize the mean-squared error, the actual implementation of these methods may be prohibitive complex for a channel equivalent to the one that is being analyzed in this document. By assuming that the fading at the N subcarriers are independent, it is assumed that there are N degrees of freedom in one form or another. This channel assumption could imply that there are N resolvable paths in a DS-CDMA rake receiver. It could mean that there are N taps in the impulse response of the channel and a very large number of states in a Viterbi decoder for large N . It could also mean there are N taps in a LMS implementation of a Wiener filter.

In the analysis, three equalization techniques will be evaluated: Equal Gain Combining (EGC), Maximal Ratio Combining (MRC) and Controlled Equalization (CE). These techniques may be associated with classical diversity theory as they involved multiplying each copy of the signal by some gain factor as shown in Fig. 3. As it can be seen from Eq. (17), each of the equalization techniques will affect the distribution of the noise component differently. In Appendix A, the statistical characteristics of the noise for the different equalization techniques are discussed.

3.9.1 EGC

With EGC, the gain factor of the i th subcarrier is chosen to be

$$d_{0,i} = 1, \quad (20)$$

that is, this technique does not attempt to equalize the effect of the channel distortion in any way. This technique may be desirable for its simplicity as the receiver does not require the estimation of the channel's transfer function. Using this scheme, the decision variable of Eq. (18) is given as

$$v_o = a_0[k] \sum_{i=0}^{N-1} \rho_{0,i} + \sum_{m=1}^{M-1} a_m[k] \sum_{i=0}^{N-1} c_m[i] c_0[i] \rho_{m,i} \cos \bar{\theta}_{m,i} + \eta \quad (21)$$

where the noise can be approximated by a zero-mean Gaussian random with a variance of

$$\sigma_\eta^2 = N \frac{N_0}{T_b}. \quad (22)$$

3.9.2 MRC

With MRC, the scheme squares the amplitude of each copy of the signal by using a gain factor for the i th subcarrier of

$$d_{0,i} = \rho_{0,i}. \quad (23)$$

The motivation behind Maximal Ratio Combining is that the components of the received signal with large amplitudes are likely to contain relatively less noise. Thus, their effect on the decision process is increased by squaring their amplitudes.

The corresponding decision variable is

$$v_o = a_o[k] \sum_{i=0}^{N-1} \rho_{0,i}^2 + \sum_{m=1}^{M-1} a_m[k] \sum_{i=0}^{N-1} c_m[i] c_o[i] \rho_{m,i} \rho_{0,i} \cos \bar{\theta}_{m,i} + \eta \quad (24)$$

where the noise can be approximated by a zero-mean Gaussian random variable with variance

$$\sigma_\eta^2 = N \frac{N_0}{T_b} E \rho_{0,i}^2. \quad (25)$$

3.9.3 Controlled Equalization

While EGC may be desirable for its simplicity and MRC for its noise combating capability, neither of these techniques directly address the interference and the exploitation of the coding at the subcarriers. As one of the goal of mobile radio communication systems is to multiplex as many users as possible to share the same resources, the channel models for these communication systems are moving from noise-limited channels to interference-limited channels. With CE, an attempt at restoring the orthogonality between users is made by normalizing the amplitudes of the subcarriers. As the orthogonality of the users is encoded in the phase of the subcarriers, this method appears to be primarily beneficial in the downlink where phase distortion for all users may be more easily corrected rather than in the uplink. For Controlled Equalization, the gain factor the i th subcarrier is

$$d_{0,i} = \frac{1}{\rho_{0,i}} u(\rho_{0,i} - \rho_{thresh}) \quad (26)$$

where $u(\rho_{0,i})$ is the unit step function. Thus, only subcarriers above a certain threshold will be equalized and retained.

This constraint is added to prevent the over amplification of subcarriers with small amplitudes that may be dominated by a noise component. Given that there are n_0 subcarriers above the threshold, the corresponding decision variable is

$$v_o|_{n_0} = a_o[k] n_0 + \sum_{m=1}^{M-1} a_m[k] \sum_j c_m[j] c_o[j] + \eta \quad (27)$$

where the inner sum of the interference term (indexed by j) is carried over the n_0 terms corresponding to the subcarriers above threshold and

$$\eta = \sum_j d_{0,j} \int_{kT_b}^{(k+1)T_b} n(t) \frac{2}{T_b} \cos(2\pi f_c t + 2\pi j \frac{F}{T_b} t + \theta_{0,j}) dt. \quad (28)$$

Equalization

The noise can be approximated by a zero-mean Gaussian random variable with a variance of

$$\sigma_{\eta|n_0}^2 = n_0 \frac{N_0}{T_b} E d_{0,j}^2. \quad (29)$$

CHAPTER 4*Analysis of the Performance of
MC-CDMA in Rayleigh and
Rician Fading Channels***4.1 Rayleigh Fading****4.1.1 Channel Model**

In this section, the scalings of the amplitude are assumed to be independent and identically distributed (IID) Rayleigh random variables of the form

$$f_{\rho_{m,i}}(\rho_{m,i}) = \frac{\rho_{m,i}}{\sigma_{m,i}^2} e^{-\left(\frac{\rho_{m,i}^2}{2\sigma_{m,i}^2}\right)} \quad (30)$$

where the indexes m and i have been added to differentiate between the m th user and the i th subcarrier. This corresponds to the case in which the LOS path from the transmitter to the receiver is obstructed by a person or an object. The phase effects, $\theta_{m,i}$ for $i = 0, 1, \dots, N-1$, introduced by the channel are assumed to be IID random variables uniformly distributed on the interval $[-\pi, \pi]$ for all subcarriers. As summarized in Eq. (13), the local-mean power of one subcarrier is assumed to be

$$\overline{p_{m,i}} = \frac{1}{2} E \rho_{m,i}^2 = \sigma_{m,i}^2$$

with each user having a total local-mean power of $\overline{p_m} = N \overline{p_{m,i}}$.

4.1.2 Uplink

For uplink transmissions, we will consider only EGC and MRC for the following reason. As mentioned above, for uplink transmissions, phase correction is not simultaneously applied to the interference when it is applied to the desired signal. Examining the interference component of the decision variable for EGC and MRC in Eq. (21) and in Eq. (24), the phase distortion results in the multiplicative term $\cos \bar{\theta}_{m,i}$. This term can add a phase of 0 or π depending on the value of $\bar{\theta}_{m,i}$ which happens to be random. As the code is encoded in the phase, the phase distortion will randomize the phase and consequently cancel the effect of the orthogonal coding unless predistortion is applied in the transmitters of the interfering signals.

4.1.2.1 EGC

For EGC in the uplink, as explained below, the interference term

$$\beta_{int} = \sum_{m=1}^{M-1} a_m[k] \sum_{i=0}^{N-1} c_m[i] c_0[i] \rho_{m,i} \cos \bar{\theta}_{m,i} \quad (31)$$

is a Gaussian r.v. Since the in-phase component of a Rayleigh random variable, $\rho_{m,i} \cos \bar{\theta}_{m,i}$, is Gaussian and $a_m[k] c_m[i] c_0[i] \in \{-1, 1\}$, β_{int} consists of the sum of $(M-1) \times N$ iid Gaussian r.v.'s. Thus, β_{int} is Gaussian with a mean and variance (as calculated in Appendix B) of

$$E\beta_{int} = 0 \quad \sigma_{\beta_{int}}^2 = (M-1)\bar{p}_m. \quad (32)$$

Examining Eq. (21), the probability of making a decision error conditioned on the amplitudes of the desired signal, $\{\rho_{0,i}\}_{i=0}^{N-1}$, and the local-mean interference power, $\sigma_{\beta_{int}}^2$, given $a_0[k] = -1$ is

$$Pr(\text{error} | \{\rho_{0,i}\}_{i=0}^{N-1}, \sigma_{\beta_{int}}^2) = Pr\left(\sum_{i=0}^{N-1} \rho_{0,i} < \beta_{int} + \eta\right). \quad (33)$$

Note that since $a_m[k]$ is assumed to take on values of 1 and -1 with equal probability, the average probability of making a decision error is equal to the bit error rate (BER). As the interference term and the noise term are independent and Gaussian, the sum to the right of the inequality has a zero-mean Gaussian distribution with a variance equal to the sum of their variances. Using this observation, the probability of a decision error can be found to be

$$Pr(\text{error} | \{\rho_{0,i}\}_{i=0}^{N-1}, \sigma_{\beta_{int}}^2) = \int_{\sum_{i=0}^{N-1} \rho_{0,i}}^{\infty} \frac{1}{\sqrt{2\pi(\sigma_{\beta_{int}}^2 + \sigma_n^2)}} e^{\left\{-\frac{y^2}{2(\sigma_{\beta_{int}}^2 + \sigma_n^2)}\right\}} dy. \quad (34)$$

Performing a change of variables results in

$$Pr(\text{error} | \{\rho_{0,i}\}_{i=0}^{N-1}, \bar{p}_m) = \frac{1}{2} \operatorname{erfc} \left(\frac{\sqrt{\frac{1}{2} \left(\sum_{i=0}^{N-1} \rho_{0,i} \right)^2}}{\sqrt{(M-1)\bar{p}_m + \frac{NN_0}{T_b}}} \right) \quad (35)$$

where the complementary error function is defined to be

$$\operatorname{erfc}(x) = \frac{2}{\sqrt{\pi}} \int_x^{\infty} e^{-t^2} dt. \quad (36)$$

To obtain an expression for the average probability of making a decision error, Eq. (35) must be averaged over the distribution of the instantaneous amplitudes $\{\rho_{0,i}\}_{i=0}^{N-1}$.

Finding the distribution of the sum of iid Rayleigh random variables

$$\rho_0 = \sum_{i=0}^{N-1} \rho_{0,i} \quad (37)$$

has historically been a difficult problem. In [16], Beaulieu offers an infinite series representation of this sum that has some computational advantages. In this paper, three approximations of the distribution will be compared: a Law of Large Numbers (LLN) approximation, a small parameter approximation [16], and a Central Limit Theorem (CLT) approximation.

1. LLN

In the limiting case of a large number of subcarriers, $\sum_{i=0}^{N-1} \rho_{0,i}$ can be approximated by the LLN to be the constant $NE\rho_{0,i}$.

The advantage of using the LLN is that it requires low computational complexity. Using the LLN simplifies the expression for the probability of error to

$$Pr(\text{error} | E\rho_0, \bar{p}_m) \cong \frac{1}{2} \operatorname{erfc} \left(\frac{\sqrt{\frac{1}{2} N^2 E^2 \rho_{0,i} T_b}}{\sqrt{(M-1)\bar{p}_m T_b + NN_0}} \right). \quad (38)$$

Applying the statistical properties of Rayleigh distributions given in Eq. (4), the probability of error simplifies to

$$Pr(\text{error} | \bar{p}_0, \bar{p}_m) \cong \frac{1}{2} \operatorname{erfc} \left(\frac{\sqrt{\frac{\pi}{4} \frac{\bar{p}_0 T_b}{(M-1)\frac{\bar{p}_m}{N} T_b + N_0}}}{\sqrt{(M-1)\frac{\bar{p}_m}{N} T_b + N_0}} \right). \quad (39)$$

2. Small Argument Approximation

For small values of ρ_0 , the distribution of ρ_0 can be approximated by

$$f(\rho_0 | \bar{p}_0) = \frac{\rho_0^{2N-1} e^{-\frac{\rho_0^2}{2b}}}{2^{N-1} b^N (N-1)!} \quad (40)$$

where $b = \frac{\bar{p}_0}{N} [(2N-1)!!]^{1/N}$. In contrast to the LLN approximation, ρ_0 is considered to be a random variable instead of a deterministic constant. Thus, the average probability of making a decision error may be approximated by averaging over Eq. (40) to yield

$$Pr(\text{error} | \bar{p}_0, \bar{p}_m) \cong \int_0^\infty \frac{\rho_0^{2N-1} e^{-\frac{\rho_0^2}{2b}}}{2^{N-1} b^N (N-1)!} \frac{1}{2} \text{erfc} \left(\sqrt{\frac{\frac{1}{2} \rho_0^2 T_b}{(M-1) \bar{p}_m T_b + NN_0}} \right) d\rho_0. \quad (41)$$

3. CLT

A third possible approximation can be obtained by applying the CLT for the limiting case of large N. Using the CLT results in a BER of

$$Pr(\text{error} | \bar{p}_0, \bar{p}_m) \cong \int_{-\infty}^\infty \frac{1}{\sqrt{2\pi\sigma_{\rho_0}^2}} e^{-\frac{(\rho_0 - \mu_{\rho_0})^2}{2\sigma_{\rho_0}^2}} \frac{1}{2} \text{erfc} \left(\sqrt{\frac{\frac{1}{2} \rho_0^2 T_b}{(M-1) \bar{p}_m T_b + NN_0}} \right) d\rho_0 \quad (42)$$

where $\mu_{\rho_0} = \sqrt{\frac{\pi}{2} N \bar{p}_0}$ and $\sigma_{\rho_0}^2 = (2 - \frac{\pi}{2}) \bar{p}_0$. This expression may be simplified by exchanging the order of the integrals to yield

$$Pr(\text{error} | \bar{p}_0, \bar{p}_m) \cong \frac{1}{2} \text{erfc} \left(\sqrt{\frac{\frac{\pi}{4} \bar{p}_0 T_b}{(2 - \frac{\pi}{2}) \frac{\bar{p}_0}{N} T_b + (M-1) \frac{\bar{p}_m}{N} T_b + N_0}} \right). \quad (43)$$

Thus, the randomness of the desired signals' amplitudes may be reflected as an addition to the power of the interference and noise and consequently is a more conservative approximation than the LLN approximation.

4.1.2.2 MRC

For MRC, the interference component is given as

$$\beta_{int} = \sum_{m=1}^{M-1} a_m[k] \sum_{i=0}^{N-1} c_m[i] c_0[i] \rho_{m,i} \rho_{0,i} \cos \tilde{\theta}_{m,i}. \quad (44)$$

Comparing Eq. (44) with Eq. (31), it can be seen that for MRC and EGC, the interference components have similar forms. Thus, the analysis for MRC should follow the analysis of EGC. Since β_{int} consists of $(M-1) \times N$ iid r.v.'s with respect to m and i , it can be approximated by a zero-mean Gaussian r.v. with a variance as determined in Appendix B of

$$\sigma_{\beta_m}^2 = 2 \frac{(M-1)}{N} \bar{p}_m \bar{p}_0. \quad (45)$$

Using Eq. (24) Eq. (25) Eq. (45), the conditioned instantaneous BER for MRC can be calculated to be

$$Pr(error | \{p_{0,i}\}_{i=0}^{N-1}, \bar{p}_0, \bar{p}_m) = \frac{1}{2} \operatorname{erfc} \left(\sqrt{\frac{\frac{1}{2} \left(\sum_{i=0}^{N-1} p_{0,i}^2 \right)^2}{2 \frac{(M-1)}{N} \bar{p}_m \bar{p}_0 + \frac{2\bar{p}_0 N_0}{T_b}}} \right). \quad (46)$$

1. Exact

Fortunately, the distribution of the sum of exponentially distributed random variables $r = \sum_{i=0}^{N-1} \frac{1}{2} p_{0,i}^2$ is known to have the gamma distribution which has the following closed form distribution

$$f(r | \bar{p}_0) = \frac{1}{\bar{p}_{0,i} (N-1)!} \left(\frac{r}{\bar{p}_{0,i}} \right)^{N-1} e^{-\frac{r}{\bar{p}_{0,i}}}. \quad (47)$$

Unconditioning Eq. (46) over Eq. (47) results in the following exact expression for the average probability of error using MRC

$$Pr(error | \bar{p}_0, \bar{p}_m) = \int_0^{\infty} \frac{1}{\bar{p}_{0,i} (N-1)!} \left(\frac{r}{\bar{p}_{0,i}} \right)^{N-1} e^{-\frac{r}{\bar{p}_{0,i}}} \frac{1}{2} \operatorname{erfc} \left(\sqrt{\frac{r^2 T_b}{\frac{(M-1)}{N} \bar{p}_m \bar{p}_0 T_b + \bar{p}_0 N_0}} \right) dr. \quad (48)$$

2. LLN

Using Eq. (48) as a basis of comparison, the expressions of the probability of error for the LLN and CLT will be included so that the effectiveness of the EGC approximations can be judged. Using the LLN, the probability of error is given as

$$Pr(error | \bar{p}_0, \bar{p}_m) \cong \frac{1}{2} \operatorname{erfc} \left(\sqrt{\frac{\bar{p}_0 T_b}{\frac{(M-1)}{N} \bar{p}_m T_b + N_0}} \right). \quad (49)$$

3. CLT

Using the CLT approximation with $\mu = 2\bar{p}_0$ and $\sigma^2 = 4 \frac{\bar{p}_0}{N}$, the probability of error can be found to be

$$Pr(error | \bar{p}_0, \bar{p}_m) \cong \frac{1}{2} \operatorname{erfc} \left(\sqrt{\frac{\bar{p}_0 T_b}{2 \frac{\bar{p}_0}{N} T_b + \frac{(M-1)}{N} \bar{p}_m T_b + N_0}} \right). \quad (50)$$

4.1.3 Downlink

As discussed earlier, downlink transmissions designated for different users arrive at one particular receiver through the same channel. Thus, in this section, we will use the notation of Eq. (14) and assume perfect phase correction for the interference. The generalized decision variable given in Eq. (18) simplifies to

$$v_o = a_o[k] \sum_{i=0}^{N-1} \rho_{0,i} d_{0,i} + \sum_{m=1}^{M-1} \sum_{i=0}^{N-1} a_m[k] c_m[i] c_o[i] \rho_{0,i} d_{0,i} + \eta. \quad (51)$$

Note that in contrast to the uplink, the sign reversals due to phase distortions are no longer present in the interference term. Thus, the effect of the subcarrier coding is not invalidated by the channel and can be included in the analysis. Let

$$Q[i] = c_l[i] c_m[i]. \quad (52)$$

Note that the orthogonality of the codes described in Eq. (8)

$$\sum_{i=0}^{N-1} Q[i] = 0 \quad (53)$$

for $l \neq m$ and the fact that $Q[i] \in \{-1, 1\}$ imply that the set $A = \{Q[i]\}_{i=0}^{N-1}$ consists of exactly $\frac{N}{2}$ elements that are equal to "1" and exactly $\frac{N}{2}$ elements that equal to "-1". Let the elements of set A that are equal to "1" be indexed by a_j and the elements that are equal to "-1" be indexed by b_j for $j = 0, 1, \dots, \frac{N}{2} - 1$ such that

$$\begin{aligned} Q[a_j] &= 1 & Q[b_j] &= -1 \\ \{a_j\} \cup \{b_j\} &= \{0, 1, \dots, N-1\} \end{aligned} \quad (54)$$

Using this notation, the generalized decision variable in the downlink may be written as

$$v_o = a_o[k] \sum_{i=0}^{N-1} \rho_{0,i} d_{0,i} + \sum_{m=1}^{M-1} a_m[k] \left[\sum_{j=0}^{\frac{N}{2}-1} \rho_{0,a_j} d_{0,a_j} - \sum_{j=0}^{\frac{N}{2}-1} \rho_{0,b_j} d_{0,b_j} \right] + \eta. \quad (55)$$

4.1.3.1 EGC

Using Eq. (55), the decision variable for EGC is given as

$$v_o = a_o[k] \sum_{i=0}^{N-1} \rho_{0,i} + \sum_{m=1}^{M-1} a_m[k] \left[\sum_{j=0}^{\frac{N}{2}-1} \rho_{0,a_j} - \sum_{j=0}^{\frac{N}{2}-1} \rho_{0,b_j} \right] + \eta \quad (56)$$

where the interference now has a variance of

$$\sigma_{p_m}^2 = 2(M-1) \left[1 - \frac{\pi}{4} \right] \bar{p}_0. \quad (57)$$

Following an analysis similar to that of the uplink and using Eq. (22) and Eq. (57), the average BER for EGC in the downlink can be obtained for the following approximations

1. LLN

$$Pr(error|\bar{p}_0) \cong \frac{1}{2} \operatorname{erfc} \left(\sqrt{\frac{\pi}{4} \frac{\bar{p}_0 T_b}{2 \frac{(M-1)}{N} \left[1 - \frac{\pi}{4}\right] \bar{p}_0 T_b + N_0}} \right) \quad (58)$$

2. Small Argument

$$Pr(error|\bar{p}_0) \cong \int_0^{\infty} \frac{\rho_0^{2N-1} e^{-\frac{\rho_0^2}{2b}}}{2^{N-1} b^N (N-1)!} \frac{1}{2} \operatorname{erfc} \left(\sqrt{\frac{\frac{1}{2} \rho_0^2 T_b}{2(M-1) \left(1 - \frac{\pi}{4}\right) \bar{p}_0 T_b + NN_0}} \right) d\rho_0 \quad (59)$$

3. CLT

With $\mu_{\rho_0} = \sqrt{\frac{\pi}{2} N \bar{p}_0}$ and $\sigma_{\rho_0}^2 = (2 - \frac{\pi}{2}) \bar{p}_0$, the BER can be expressed as

$$Pr(error|\bar{p}_0) \cong \frac{1}{2} \operatorname{erfc} \left(\sqrt{\frac{\pi}{4} \frac{\bar{p}_0 T_b}{2 \frac{M}{N} \left[1 - \frac{\pi}{4}\right] \bar{p}_0 T_b + N_0}} \right). \quad (60)$$

Comparing Eq. (58) with Eq. (60), it can be seen that using the CLT approximation is more conservative, resulting in "1" additional interfering power compared to the LLN approximation.

4.1.3.2 MRC

The decision variable for MRC in the downlink is

$$v_o = a_o[k] \sum_{i=0}^{N-1} \rho_{0,i}^2 + \sum_{m=1}^{M-1} a_m[k] \left[\sum_{j=0}^{\frac{N}{2}-1} \rho_{0,a_j}^2 - \sum_{j=0}^{\frac{N}{2}-1} \rho_{0,b_j}^2 \right] + \eta \quad (61)$$

where from Appendix B the interference has a variance of

$$\sigma_{p_{int}}^2 = \left(\frac{M-1}{N}\right) 4\bar{p}_0^2. \quad (62)$$

Following an analysis similar to that of the uplink and using Eq. (25) and Eq. (62), the average BER for MRC in the downlink can be obtained for the following approximations

1. Exact

$$Pr(error|\bar{p}_0) = \int_0^{\infty} \frac{1}{\bar{p}_{0,i} (N-1)!} \left(\frac{r}{\bar{p}_{0,i}}\right)^{N-1} e^{-\frac{r}{\bar{p}_{0,i}}} \frac{1}{2} \operatorname{erfc} \left(\sqrt{\frac{r^2 T_b}{2 \frac{(M-1)}{N} \bar{p}_0 T_b + \bar{p}_0 N_0}} \right) dr \quad (63)$$

2. LLN

$$Pr(\text{error}|\bar{p}_0) \cong \frac{1}{2} \operatorname{erfc} \left(\sqrt{\frac{\bar{p}_0 T_b}{2 \frac{(M-1) \bar{p}_0 T_b + N_0}{N}}} \right) \quad (64)$$

3. CLT

Using the CLT approximation with $\mu = 2\bar{p}_0$ and $\sigma^2 = 4 \frac{\bar{p}_0^2}{N}$, the probability of error can be found to be

$$Pr(\text{error}|\bar{p}_0) \cong \frac{1}{2} \operatorname{erfc} \left(\sqrt{\frac{\bar{p}_0 T_b}{2 \frac{M-1}{N} \bar{p}_0 T_b + N_0}} \right). \quad (65)$$

4.1.3.3 Controlled Equalization (CE)

Examining Eq. (27), the probability of making a decision error conditioned the number of subcarriers above the threshold, n_0 , and the interference component, β_{int} , given $a_0[k] = -1$ is

$$Pr(\text{error} | n_0, \beta_{int}) \cong \int_{n_0 - \beta_{int}}^{\infty} \frac{1}{\sqrt{2\pi\sigma_{\eta|n_0}^2}} e^{-\frac{x^2}{2\sigma_{\eta|n_0}^2}} dx \quad (66)$$

where the variance of the noise, $\sigma_{\eta|n_0}^2$, is given in Eq. (A-10) as

$$\sigma_{\eta|n_0}^2 = n_0 \frac{N_0}{T_b} \frac{1}{2p_{0,i}} \frac{1}{pr_{on}} E_1 \left(\frac{\rho_{thresh}^2}{2p_{0,i}} \right) \quad (67)$$

where $E_1(\rho)$ is the exponential integral defined as

$$E_1(\rho) = \int_{\rho}^{\infty} \frac{e^{-t}}{t} dt \quad (68)$$

and the probability that a subcarrier is above the threshold for Rayleigh fading is

$$pr_{on} = e^{-\frac{\rho_{thresh}^2}{2p_{0,i}}}. \quad (69)$$

The distribution of the number of subcarriers above the threshold, n_0 , is described by the following binomial distribution

$$p_{n_0}(n_0) = \binom{N}{n_0} \{pr_{on}\}^{n_0} \{1 - pr_{on}\}^{N-n_0} \quad (70)$$

for $n_0 = 0, 1, 2, \dots, N$. As mentioned earlier, note that the orthogonality of the codes, given by the following condition

$$\sum_{i=0}^{N-1} c_m[i] c_o[i] = N\delta_{m,0}. \quad (71)$$

imply that half of the inner products, $c_m[i] c_o[i]$, are positive while the other half are negative. Denote the inner sum of the interference term of Eq. (27) by

$$\Sigma_m = \sum_j c_m [j] c_0 [j]. \quad (72)$$

Using this notation, the distribution of the inner sum given that there are n_0 subcarriers above threshold is

$$P_{\Sigma_m | n_0}(\Sigma_m | n_0) = \frac{\binom{N/2}{(n_0 + \Sigma_m)/2} \binom{N/2}{(n_0 - \Sigma_m)/2}}{\binom{N}{n_0}} \quad (73)$$

where $-\min\{n_0, N - n_0\} \leq \Sigma_m \leq \min\{n_0, N - n_0\}$ and Σ_m can only assume even (odd) values if n_0 is even (odd). The exact distribution of the interference term, β_{int} , given n_0 depends on the spreading code, $\{c_m[i]\}$ for $i = 0, 1, \dots, N-1$. In this analysis, it is assumed that each of the inner sums acts as an independent r.v., and that the pdf of the interference is given as the convolution of the pdfs of Σ_m for $m = 1, 2, \dots, M-1$. Combining the results given above yield the following expression for the bit error rate

$$BER \cong \sum_{n_0=0}^N p_{n_0}(n_0) \sum_{\beta_{int}} P_{\beta_{int} | n_0}(\beta_{int} | n_0) \frac{1}{2} \operatorname{erfc} \left(\frac{n_0 - \beta_{int}}{\sqrt{2} \sigma_{\eta | n_0}} \right). \quad (74)$$

4.2 Rician Fading

In an indoor environment, the direct path from the transmitter, which most likely is located on the ceiling, to the receiving terminal is usually unobstructed. Thus, the Rician distribution given in Eq. (5) is more appropriate when describing of the amplitude scalings, $\rho_{m,i}$ of the channel. To conform to the multi-carrier and multi-user notation, the Rician distribution is rewritten as

$$f_{\rho_{m,i}}(\rho_{m,i}) = \frac{\rho_{m,i}}{\sigma_{m,i}^2} e^{-\frac{\rho_{m,i}^2 + b_0^2}{2\sigma_{m,i}^2}} I_0 \left(\frac{b_0 \rho_{m,i}}{\sigma_{m,i}^2} \right) \quad (75)$$

where the indexes i and m have been added to differentiate between the i th subcarrier at the frequency $f_0 + F \frac{i}{T_b}$ and the m th user. As the notation suggests, the dominant LOS component, b_0 , is assumed to equal for all subcarriers and all users. With BPSK modulation, the power of the LOS component for "1" subcarrier is $\frac{1}{2} b_0^2$. The scattered power, $\sigma_{m,i}^2$, is also assumed to be equal with respect to user m and subcarrier i . As a consequence, the Rician K-factor given in Eq. (6) and rewritten here using the user/subcarrier notation

$$K = \frac{b_0^2}{2\sigma_{m,i}^2}, \quad (76)$$

is equal for users and subcarriers. The mean given in Eq. (7) can be rewritten as

$$E\rho_{m,i} = e^{-K/2} \sqrt{\frac{\pi}{2(K+1)}} \overline{p_{0,i}} \left[(1+K) I_0\left(\frac{K}{2}\right) + K I_1\left(\frac{K}{2}\right) \right]. \quad (77)$$

Assuming BPSK modulation, the local-mean power of the i th subcarrier of the m th user consisting of a contribution from the scattered component and the LOS component is defined to be

$$\overline{p_{m,i}} = E \left[\rho_{m,i} \cos \left(2\pi f_c t + 2\pi i \frac{F}{T_b} t + \theta_{m,i} \right) \right]^2 = \frac{1}{2} E \rho_{m,i}^2 = \sigma_{m,i}^2 + \frac{1}{2} b_0^2. \quad (78)$$

In terms of the Rician K -factor and the local-mean power, the power of the dominant and scattered components can be rewritten as

$$\frac{1}{2} b_0^2 = \frac{K}{K+1} \overline{p_{m,i}} \quad \sigma_{m,i}^2 = \frac{\overline{p_{m,i}}}{K+1}. \quad (79)$$

Consequently, the Rician pdf may be rewritten in terms of the K -factor as

$$f_{\rho_{m,i}}(\rho_{m,i} | K, \overline{p_{m,i}}) = (K+1) e^{-K} \frac{\rho_{m,i}}{\overline{p_{m,i}}} e^{-\frac{K+1}{2\overline{p_{m,i}}} \rho_{m,i}^2} I_0 \left(\rho_{m,i} \sqrt{\frac{2K(K+1)}{\overline{p_{m,i}}}} \right). \quad (80)$$

4.2.1 Uplink

The method for obtaining the BER with Rician fading is identical to that of Rayleigh fading with the same decision variables being used. The only factors that change in the expressions are the replacement of the statistical properties of Rayleigh fading with Rician fading. The calculation of the statistical properties of the interference assuming Rician fading are included in Appendix B. To obtain the average BER, the conditional expressions that are obtained must be averaged over the sum of Rician r.v.'s or of Rician-squared r.v.'s. Again, the difficulty of finding closed form expressions for the distribution of these r.v.'s are encountered. Again, the LLN and CLT will be used to approximate the average BER. While it is theoretically possible to synchronize the transmitters in time so that the LOS components will maintain their orthogonality and cancel out of the decision variable, it can be shown that this scenario would require a time synchronization of within T_b/N which may not be feasible for high bit rates or large N . Thus, this case is not considered.

4.2.1.1 EGC

With EGC in a Rician fading channel, the variance of the interference is given in Appendix B as

$$\sigma_{\beta_{int}}^2 = (M-1) \overline{p_m}. \quad (81)$$

The average BER for the LLN and CLT approximations are

1. LLN

$$Pr(\text{error} | \bar{p}_0, K) \cong \frac{1}{2} \operatorname{erfc} \left(\sqrt{\frac{\gamma \bar{p}_0 T_b}{\left(\frac{M-1}{N}\right) \bar{p}_m T_b + N_0}} \right) \quad (82)$$

where

$$\gamma = \frac{\pi}{4} \left(\frac{e^{-K}}{K+1} \right) \left[(1+K) I_0 \left(\frac{K}{2} \right) + K I_1 \left(\frac{K}{2} \right) \right]^2. \quad (83)$$

2.

Applying the CLT with $\mu_{p_0} = \sqrt{2N\gamma\bar{p}_0}$ and $\sigma_{p_0}^2 = 2(1-\gamma)\bar{p}_0$ results in

$$Pr(\text{error} | \bar{p}_0, \bar{p}_m, K) \cong \frac{1}{2} \operatorname{erfc} \left(\sqrt{\frac{\bar{p}_0 T_b}{2[1-\gamma] \frac{\bar{p}_0}{N} T_b + \frac{M-1}{N} \bar{p}_m T_b + N_0}} \right). \quad (84)$$

4.2.1.2 MRC

With MRC in the uplink of a Rician fading channel, the variance of the interference is given in Appendix B as

$$\sigma_{\beta_{int}}^2 = 2 \frac{(M-1)}{N} \bar{p}_m \bar{p}_0. \quad (85)$$

The BER expressions that result are as follows.

1. LLN

$$Pr(\text{error} | \bar{p}_0, K) \cong \frac{1}{2} \operatorname{erfc} \left(\sqrt{\frac{\bar{p}_0 T_b}{\left(\frac{M-1}{N}\right) \bar{p}_m T_b + N_0}} \right) \quad (86)$$

2. CLT

Applying the CLT with $\mu_r = 2\bar{p}_0$ and $\sigma_r^2 = \frac{8K+4}{(K+1)^2} \frac{\bar{p}_0^2}{N}$ results in

$$Pr(\text{error} | \bar{p}_0, K) \cong \frac{1}{2} \operatorname{erfc} \left(\sqrt{\frac{\bar{p}_0 T_b}{\left[\frac{4K+2}{(K+1)^2} \right] \frac{\bar{p}_0}{N} T_b + \frac{M-1}{N} \bar{p}_m T_b + N_0}} \right). \quad (87)$$

4.2.2 Downlink

4.2.2.1 EGC

Approximating the interference by a Gaussian distribution, the variance of β_{int} can be determined to be

$$\sigma_{\beta_{int}}^2 = 2(M-1)(1-\gamma)\bar{p}_0. \quad (88)$$

The corresponding average BER expressions are as follows.

1. LLN

$$Pr(error|\bar{p}_0, K) \cong \frac{1}{2} \operatorname{erfc} \left(\sqrt{\frac{\gamma \bar{p}_0 T_b}{2 \left(\frac{M-1}{N}\right) [1-\gamma] \bar{p}_0 T_b + N_0}} \right) \quad (89)$$

2. CLT

Applying the CLT with $\mu_{p_0} = \sqrt{2N\gamma\bar{p}_0}$ and $\sigma_{p_0}^2 = 2(1-\gamma)\bar{p}_0$ results in

$$Pr(error|\bar{p}_0, K) \cong \frac{1}{2} \operatorname{erfc} \left(\sqrt{\frac{\gamma \bar{p}_0 T_b}{2 \frac{M}{N} [1-\gamma] \bar{p}_0 T_b + N_0}} \right). \quad (90)$$

4.2.2.2 MRC

Approximating the interference by a Gaussian distribution, the variance of β_{int} can be determined to be

$$\sigma_{\beta_{int}}^2 = \left(\frac{M-1}{N}\right) \frac{8K+4}{(K+1)^2} \bar{p}_0^2. \quad (91)$$

The resulting average BER expressions are given below.

1. LLN

$$Pr(error|\bar{p}_0, K) \cong \frac{1}{2} \operatorname{erfc} \left(\sqrt{\frac{\bar{p}_0 T_b}{\left(\frac{M-1}{N}\right) \left[\frac{4K+2}{(K+1)^2}\right] \bar{p}_0 T_b + N_0}} \right) \quad (92)$$

2. CLT

Applying the CLT with $\mu_r = 2\bar{p}_0$ and $\sigma_r^2 = \frac{8K+4}{(K+1)^2} \frac{\bar{p}_0^2}{N}$ results in

$$Pr(error|\bar{p}_0, K) \cong \frac{1}{2} \operatorname{erfc} \left(\sqrt{\frac{\bar{p}_0 T_b}{\frac{M}{N} \left[\frac{4K+2}{(K+1)^2}\right] \bar{p}_0 T_b + N_0}} \right). \quad (93)$$

Note that for all the average BER expressions obtained assuming Rician fading, the expressions for $K = 0$ reduce to that of Rayleigh fading agreeing with earlier results.

4.2.2.3 CE

With CE in a Rician fading channel, only two factors will change from the Rayleigh fading case. As mentioned in Appendix A, the variance of the noise given that there are n_0 subcarriers above threshold is now given as

$$\sigma_{\eta|n_0}^2 = n_0 \frac{N_0}{T_b} \frac{1}{2p_{0,i}} \frac{1}{pr_{on\rho_{thresh}}} \int_{\rho_{0,i} p_{0,i}}^{\infty} (K+1) e^{-K} \frac{1}{\rho_{0,i} p_{0,i}} e^{-\frac{K+1}{2p_{0,i}} \rho_{0,i}^2} I_0 \left(\rho_{0,i} \sqrt{\frac{2K(K+1)}{p_{0,i}}} \right) d\rho_{0,i} \quad (94)$$

where

$$pr_{on} = \int_{p_{thresh}}^{\infty} (K+1) e^{-\frac{K p_{0,i}}{p_{0,i}}} e^{-\frac{K+1}{2 p_{0,i}} p_{0,i}^2} I_0\left(p_{0,i} \sqrt{\frac{2K(K+1)}{p_{0,i}}}\right) dp_{0,i} \quad (95)$$

The distribution of the number of subcarriers above the threshold, n_0 , remains a binomial distribution but with a different binomial parameter, pr_{on} . The average BER expression remains the same as Eq. (74).

In the analytical section, the only closed form expressions for the average BER were obtained with MRC. In this section, approximations for the BER using the LLN and the CLT will be evaluated numerically. These results will be compared to the exact results for MRC to measure the reliability of these approximations.

5.1 Rayleigh Fading

5.1.1 Uplink

Using the expressions for the BER obtained for uplink transmissions in a Rayleigh fading channel, the average BER versus the number of co-channel interferers with a spreading factor of $N = 128$ is shown in Fig. 4. To calculate the BER, it is assumed that the local-mean power of each interferer is equal to the local-mean power of the desired signal. The SNR, which is assumed to be 10dB, is defined to be

$$SNR = \frac{\overline{P_0 T_b}}{N_0}. \quad (96)$$

Eq. (39), Eq. (41), and Eq. (43) correspond to the BER expressions for the LLN, the small argument, and the CLT approximations using EGC in the receiver. While Eq. (49) and Eq. (50) give the LLN and CLT approximations for MRC, Eq. (48) gives an exact expression for the BER. As it can be seen in Fig. 4., the approximations for MRC give relatively close results when compared to the exact result. Note that the exact results and the CLT approximation for MRC are indistinguishable. This observation indicates that the CLT approximation may be better than the LLN. For EGC, all of approximations give results that are close to the other approximations. For all approximations, it can be seen the MRC

outperforms EGC in the uplink for any number of interferers. Using the LLN expressions, the improvement in performance of MRC over EGC can be quantified by the following ratio

$$\frac{E^2 \rho}{E \rho^2} = \frac{\pi - \frac{\pi}{2^p}}{2^p} = \frac{\pi}{4} \quad (97)$$

which corresponds to -1.05 dB.

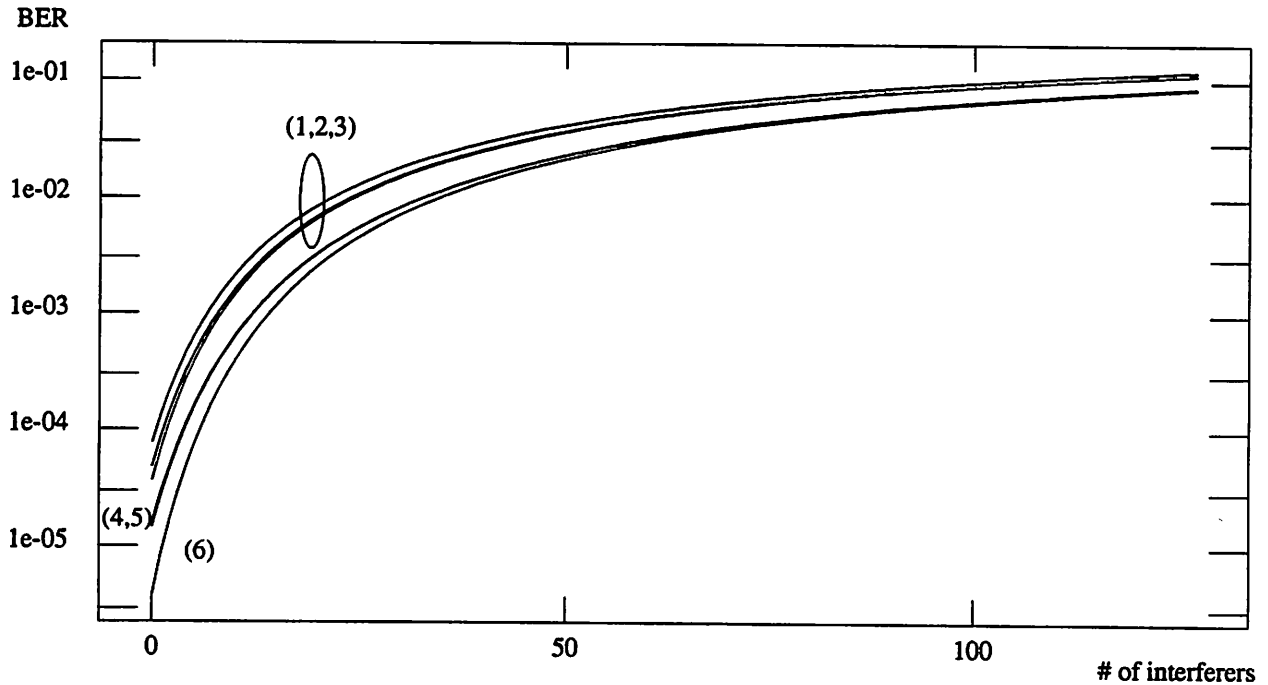


Fig. 4 BER versus the number of interferers ($m = 0, 1, \dots, 127$) for EGC in the uplink of a Rayleigh fading channel for EGC using the small argument approx. (1), CLT (2), and LLN (3) and for MRC exact (4) and approx. using CLT (5) and LLN (6). The SNR is 10dB and $N = 128$.

This difference in performance between equalization techniques can be explained as follows. Due to the phase distortion of the channel, the effects of the orthogonal codes are invalidated. Thus, for all interference loads, the receiver does not have the capability to combat the interference. Thus, it can only attempt to combat the noise. It can be shown MRC is the optimum technique in a noise-only channel. It follows that the performance for MRC is better than that of EGC in the uplink. If the acceptable BER is 10^{-3} as in some video applications, using MRC over EGC translates into an increase in CDMA user capacity of 60%.

5.1.2 Downlink

Plots of the BER for downlink transmissions over a Rayleigh fading channel using EGC and MRC are shown in Fig. 5. The SNR is assumed to be 10dB and the spreading factor is $N = 128$. Eq. (58), Eq. (59), and Eq. (60) correspond to the BER expressions for EGC using the LLN, small argument, and CLT approximations. Eq. (63), Eq. (64), and Eq. (65) correspond to the exact average BER expression and LLN and CLT approximations for MRC.

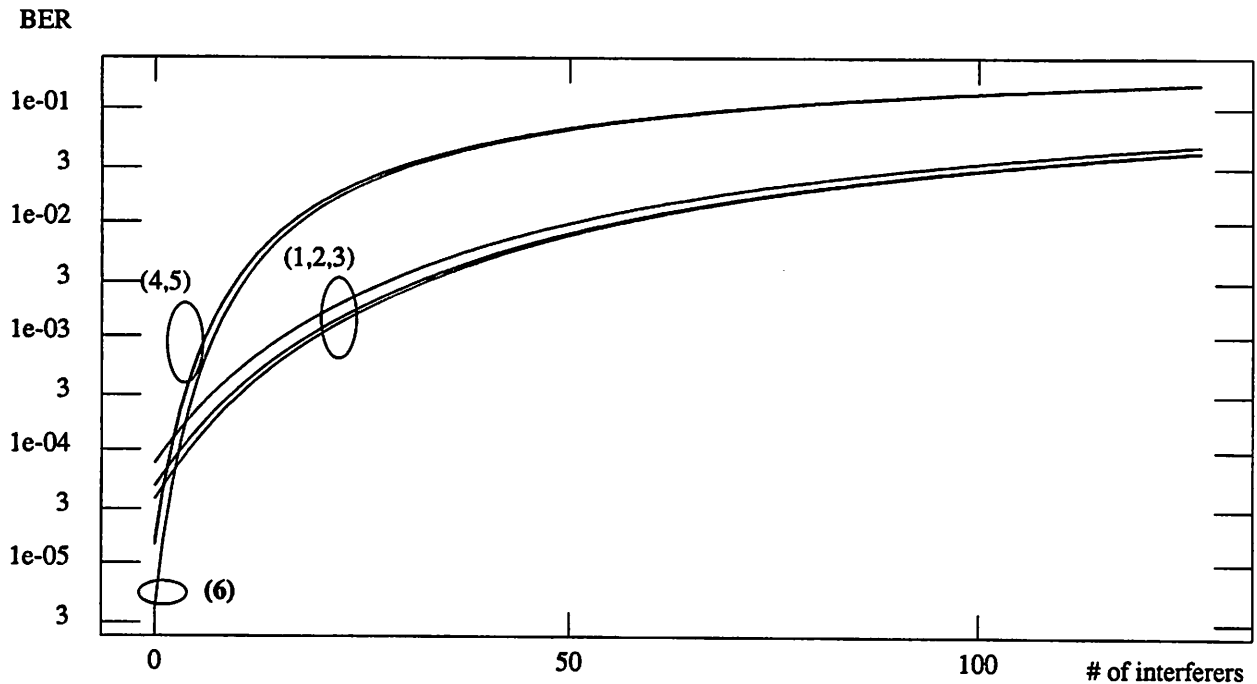


Fig. 5 BER versus the number of interferers ($m = 0, 1, \dots, 127$) in the downlink of a Rayleigh fading channel for EGC using small argument approx. (1), CLT (2), and LLN (3) and for MRC exact (4), CLT (5), and LLN (6) $N = 128$.

Examining Fig. 5, it can be seen that for a small number of users (i.e., in a noise-limited channel) MRC outperforms EGC. However, for a large number of users, EGC has a superior performance. This observation can be explained as follows. In the downlink, due to the greater degree of phase control of the interference, the orthogonal codes now have an effect on combating interference. It is desirable that the amplitudes at the subcarriers after equalization have the same amplitudes so that the interference will cancel out because of the orthogonality of the codes. With MRC, the differences between amplitudes is increased due to the squaring operation. Thus, MRC is a move away from orthogonality and consequently does not perform as well in combating interference. However, with a low number of users, the channel remains

a noise-limited channel and consequently, MRC performs better. Again, note that the exact results and the CLT approximation for MRC are indistinguishable.

In comparison to the uplink, the performance in the downlink is better when the same equalization technique is compared. Comparing the performance of EGC in the uplink to the downlink at a bit error rate of 10^{-3} , there is an increase in capacity from 8 users to 20 users in the downlink. This improvement is due to the greater degree of phase control in the downlink that allows for some of the benefits from the orthogonality of the codes to be utilized.

Plots of the BER for CE in the downlink of a Rayleigh fading channel for a SNR of 10dB and 20dB are shown in Fig. 6 and Fig. 7. The expression for the BER with CE is given in Eq. (74). The BER curves are calculated for different values of the threshold power to local-mean power (TLR) per subcarrier, which is defined to be

$$TLR = \frac{\frac{1}{2} \rho_{thresh}^2}{\overline{p_0}/N}. \quad (98)$$

Note that for large N , a SNR of 10dB results in a very small SNR at each subcarrier and a threshold power lower than the power of the noise. Plots of the performance for EGC and MRC using the LLN approximation are included for comparison. With CE, the performance also depends on the local-mean power of the desired signal which was chosen to be $\overline{p_0} = 0.1$.

As it can be seen from Fig. 6, there exists threshold levels, ρ_{thresh} , in which CE outperforms EGC and MRC for a high number of users. This observation is due to the interference combating capability of CE. Note that there exists a ρ_{thresh} such that the BER versus the number of interferers is relatively flat. At this threshold level, there are a sufficient number of subcarriers above the threshold such that orthogonality between users has been significantly restored. As the threshold level is lowered past this point, no benefit occurs since "orthogonality" has been already been achieved and only noise amplification results. For higher threshold values, the BER is affected by the number of interferers to a greater extent. Note that for all threshold levels, CE performs worse than EGC or MRC for a low number of users. This degradation is the trade-off between combating interference and combating noise. In restoring the orthogonality between users and combating interferers, the noise has also been amplified.

Although CE outperforms EGC and MRC in the downlink, the BER that is achievable with CE in a Rayleigh fading channel is still very high (on the order of 10^{-2}) for a SNR of 10dB. With a low SNR, CE suffers greatly from the amplifi-

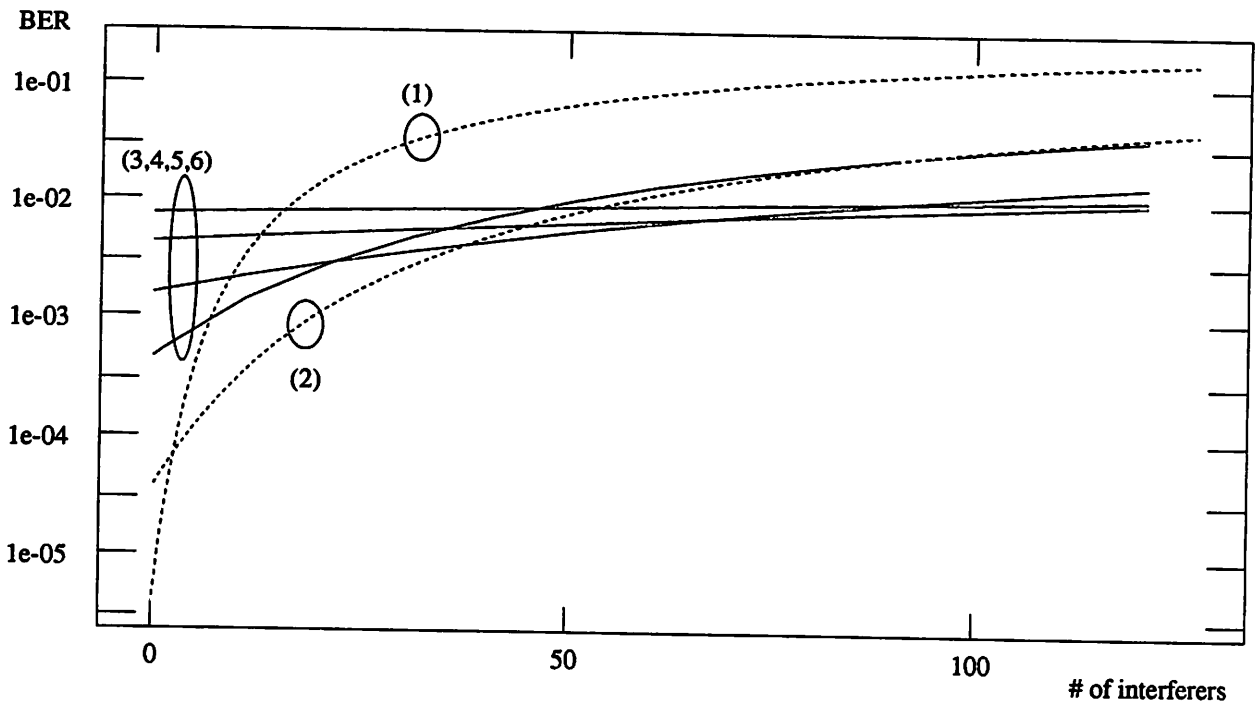


Fig. 6 BER versus the number of interferers ($m = 0, 1, \dots, 127$) in the downlink of a Rayleigh fading channel for MRC (1), EGC (2), and CE for TLR = -16.3 dB (3), TLR = -13.8 dB (4), TLR = -10.3 dB (5), and TLR = -6.8 dB. The SNR is 10dB, $\bar{p}_0 = 0.1$, and $N = 128$.

cation of the noise. If a SNR of 20dB is used, as shown in Fig. 7, acceptable BERs on the order of 10^{-8} are obtainable. With the larger SNR, CE suffers less from noise amplification.

In the downlink, the following trend is observed. For a very low number of users, MRC outperforms all equalization techniques. This observation is in agreement with theory since MRC is the optimum equalization technique in a noise-limited channel. As the number of users is increased, EGC becomes the best equalization technique out of all the methods considered. Although the interference increases, the increase is not great enough to balance the adverse effects of noise amplification that CE experiences. As the load is increased past a certain point, CE becomes the best equalization technique in the interference-limited channel.

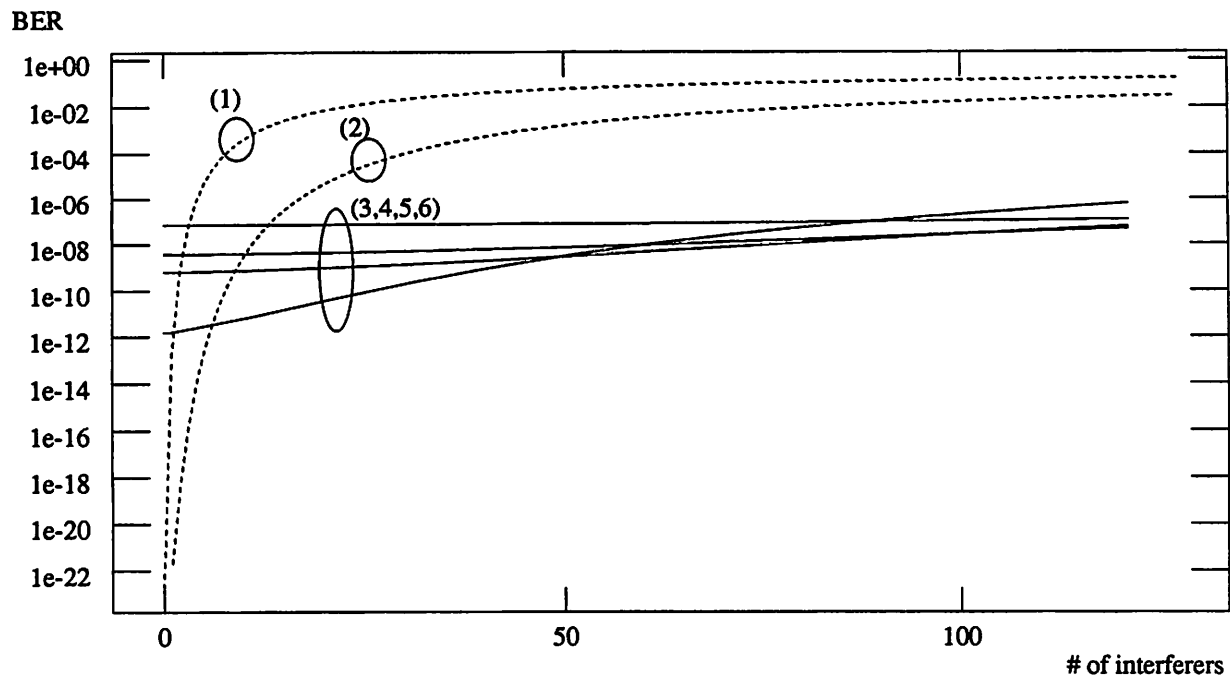


Fig. 7 BER versus the number of interferers ($m = 0, 1, \dots, 127$) in the downlink of a Rayleigh fading channel for MRC (1), EGC (2), and CE for TLR = -33.8 dB (3), TLR = -28.4 dB (4), TLR = -25.9 dB (5), and TLR = -19.9 dB. (6). The SNR is 20dB, $p_0 = 0.1$, and $N = 128$.

5.2 Rician Fading

5.2.1 Uplink

Plots of the average BER versus the number of interferers in the uplink of a Rician fading channel using EGC and MRC are shown in Fig. 8 and Fig. 9 for $K = 0, 5, 10, 15$, and 25 . The BER expressions are given in Eq. (84) and Eq. (87). Only the CLT approximations have been included to prevent the cluttering of the curves since the LLN results are almost identical. Note that without the coding of the subcarriers (due to the lack of phase control in the uplink) the K -factor has little effect in the uplink.

5.2.2 Downlink

Plots of the BER using EGC and MRC in the downlink of a Rician fading channel for various K -factors are shown in Fig. 10 and Fig. 11. A third plot that combines the curves of EGC and MRC for $K = 0$ and $K = 10$ is included so that the two frequency equalization techniques can be compared. The BER expressions for EGC using the LLN and CLT approx-

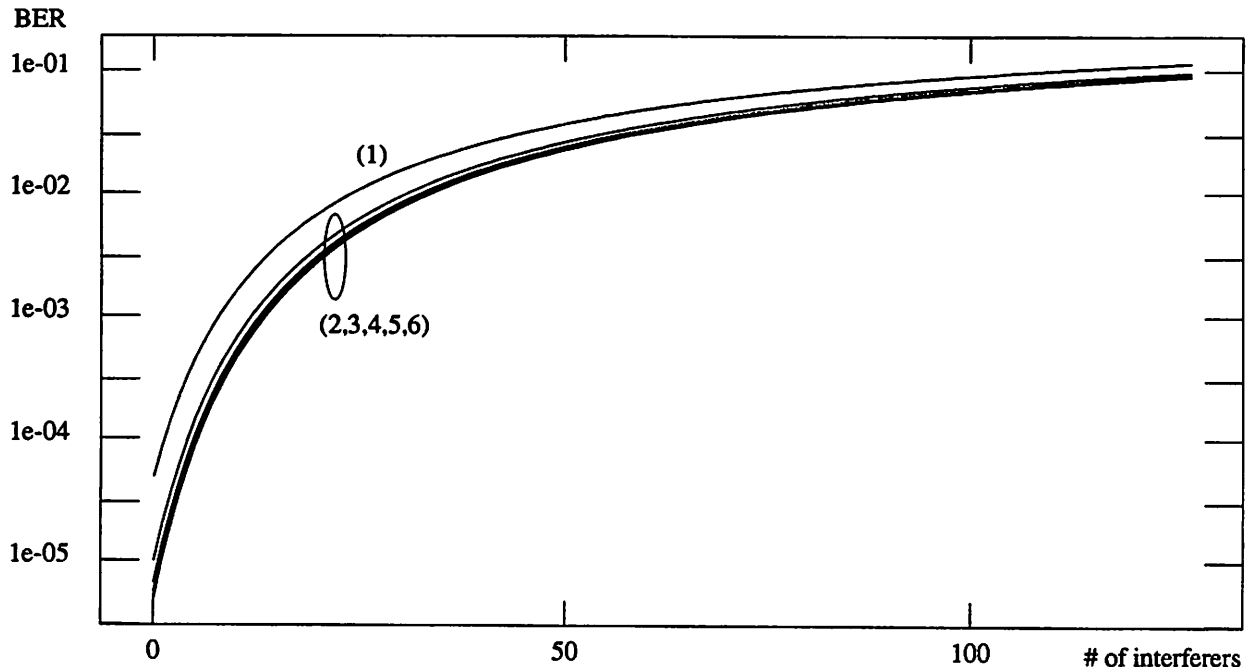


Fig. 8 BER versus the number of interferers ($m = 0, 1, \dots, 127$) in the uplink of a Rician fading channel for EGC using CLT approximations for (1) $K=0$, (2) $K=5$, (3) $K=10$, (4) $K=15$, (5) $K=20$, (6) $K=25$. $N = 128$.

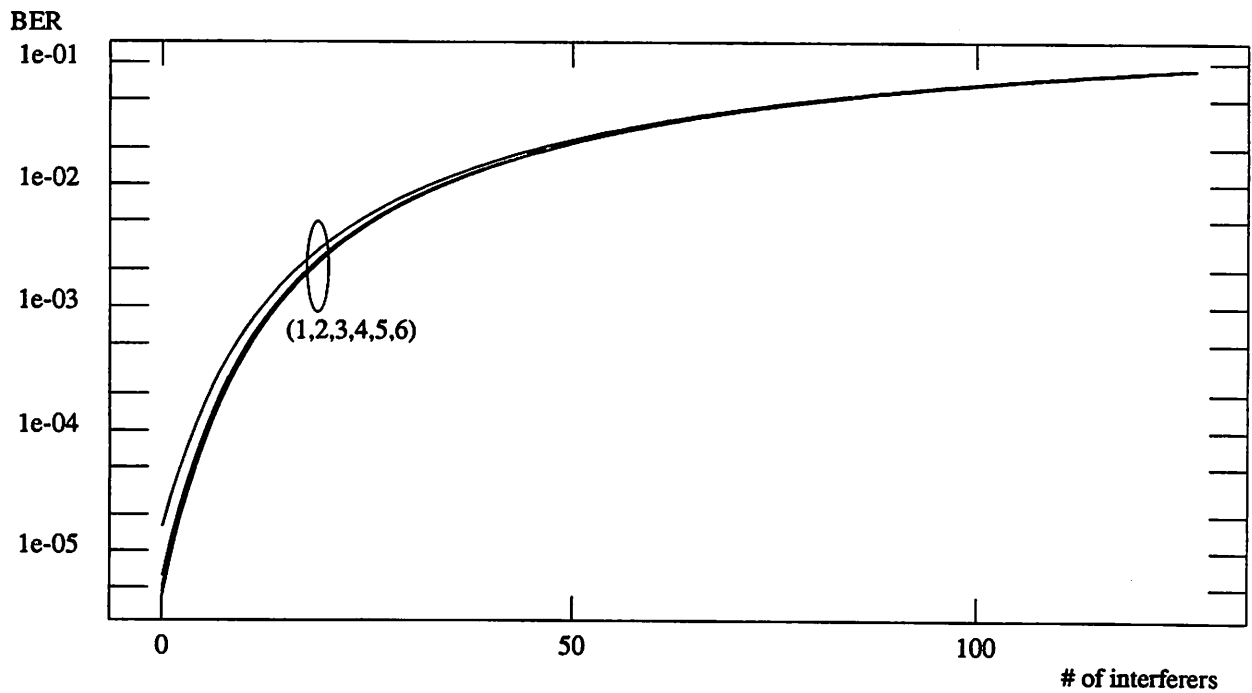


Fig. 9 BER versus the number of interferers ($m = 0, 1, \dots, 127$) in the uplink of a Rician fading channel for MRC using CLT approximations for (1) $K=0$, (2) $K=5$, (3) $K=10$, (4) $K=15$, (5) $K=20$, (6) $K=25$.

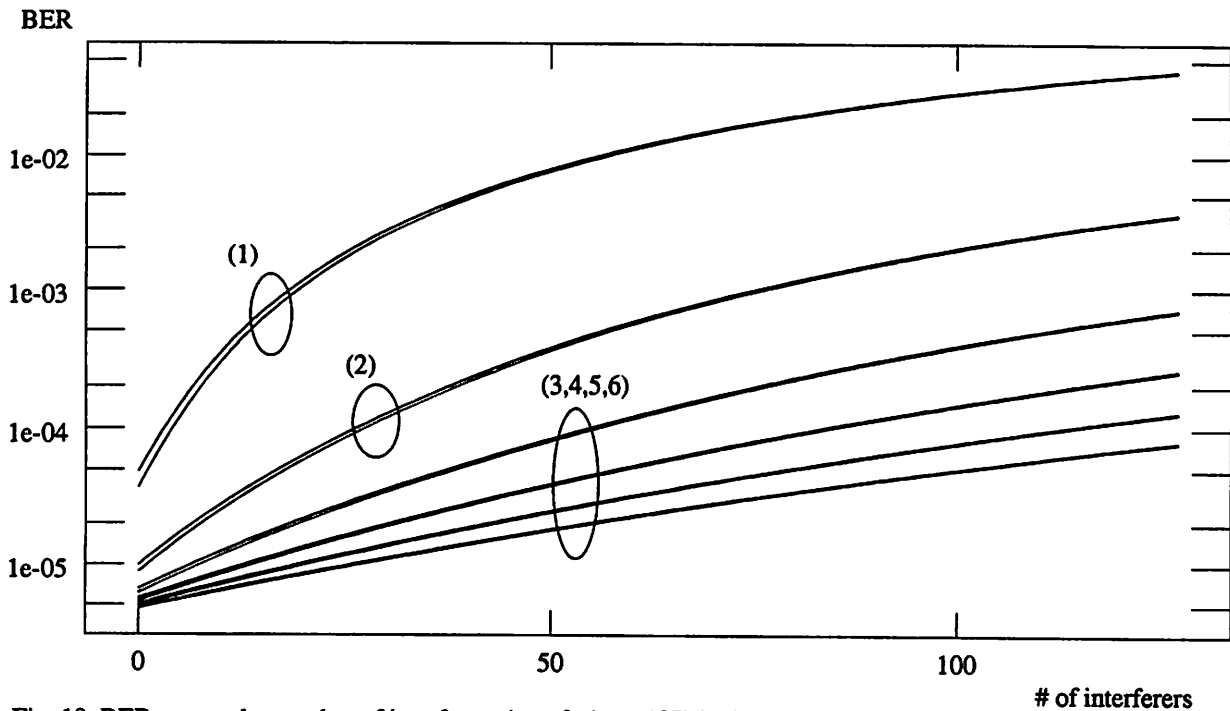


Fig. 10 BER versus the number of interferers ($m = 0, 1, \dots, 127$) in the downlink of a Rician fading channel for EGC using CLT and LLN approximations for (1) $K=0$, (2) $K=5$, (3) $K=10$, (4) $K=15$, (5) $K=20$, (6) $K=25$. $N = 128$.

imations are given in Eq. (89) and Eq. (90). The BER expressions for MRC using the LLN and the CLT approximations are given in Eq. (92) and Eq. (93).

As it can be seen from Fig. 10 and 11, the performance of the equalization techniques in the downlink improves significantly as the K -factor increases. Examining Fig. 10, it can be seen that with EGC the average BER approaches the theoretical minimum (in a noise-limited channel) for high loads as K increases. Comparing Fig. 10 and Fig. 11, it can be seen that the same trends that were observed with Rayleigh fading in the downlink, hold for all K -factors. This result can be seen more clearly in Fig. 12. In general, MRC outperforms EGC for a low number of users with EGC outperforming MRC with a large number of interferers. This observation again reflects how MRC combats noise while distorting the orthogonality of the interference. In general, the improvement in the BER curves for increasing K -factors is greater with EGC. As these curves are plotted versus the number of interferers, this agrees with intuition: EGC combats interference better than MRC.

Plots of the BER for CE in the downlink for $K = 0$, $K = 5$, and $K=10$ are shown in Figs. 6, 13, 14. The SNR was chosen to be 10dB with $\bar{p}_0 = 0.1$. These curves were generated using Eq. (74).

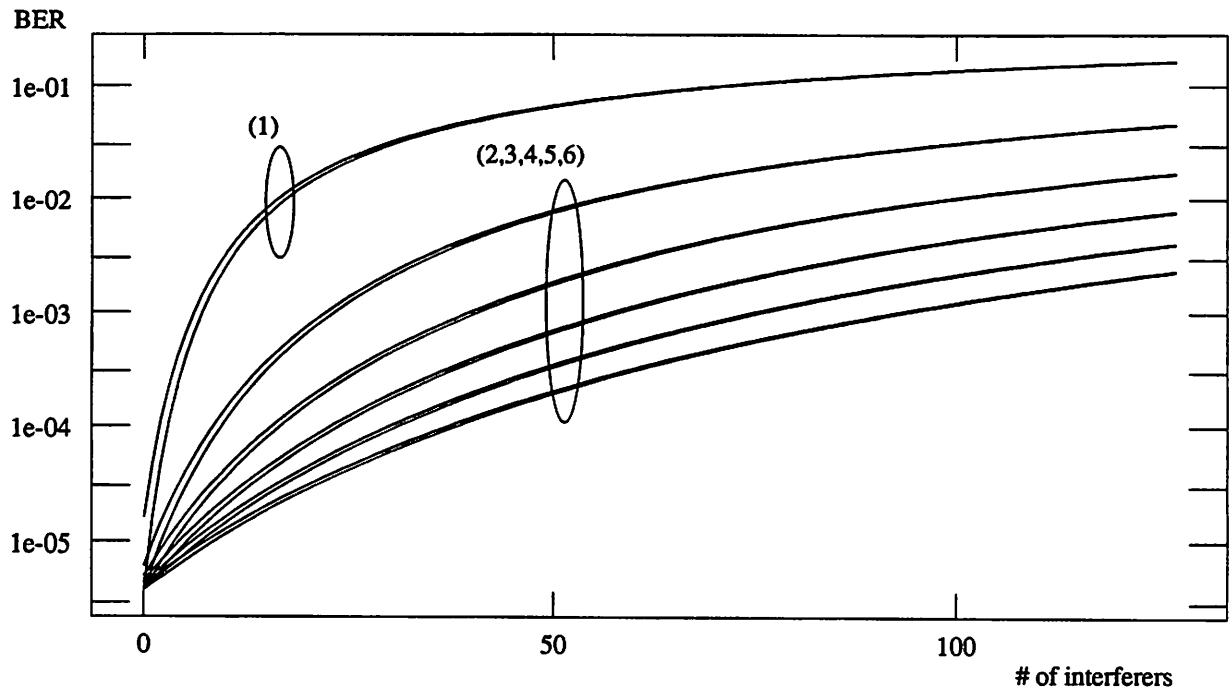


Fig. 11 BER versus the number of interferers ($m=0, 1, \dots, 127$) in the downlink of a Rician fading channel for MRC using CLT and LLN approximations for (1) $K=0$, (2) $K=5$, (3) $K=10$, (4) $K=15$, (5) $K=20$, (6) $K=25$. $N = 128$.

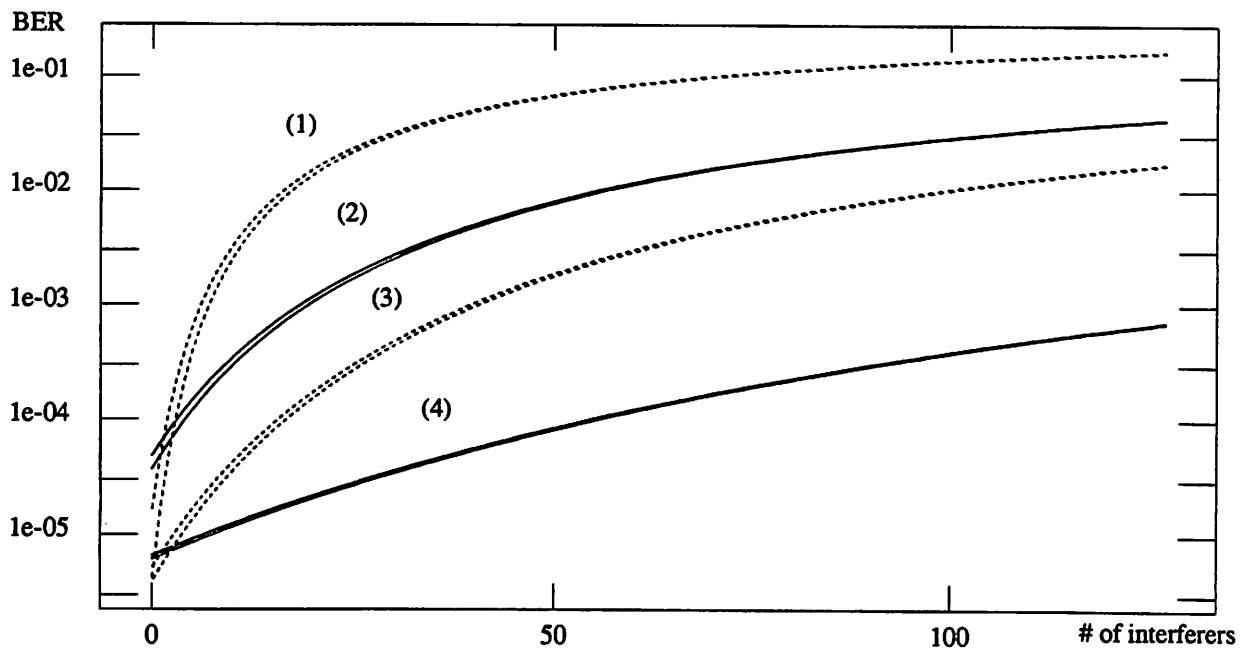


Fig. 12 BER versus the number of interferers ($m = 0, 1, \dots, 127$) for different Rician K -factors using MRC: $K=0$ (1) and $K=10$ (3) and EGC: $K=0$ (2) and $K=10$ (4). Curves are shown for both CLT and LLN approximations. The SNR is 10 dB and $N = 128$.

Numerical Results

As it can be seen from the plots, excellent performance is obtained with CE at a SNR of 10dB for $K = 10$ with $TLR = -13.8$. With this threshold, the BER versus the number of interferers is flat and close to the theoretical minimum of the noise-only channel with MRC detection. It can be seen that as the K -factor increases, the performance of CE approaches this limit.

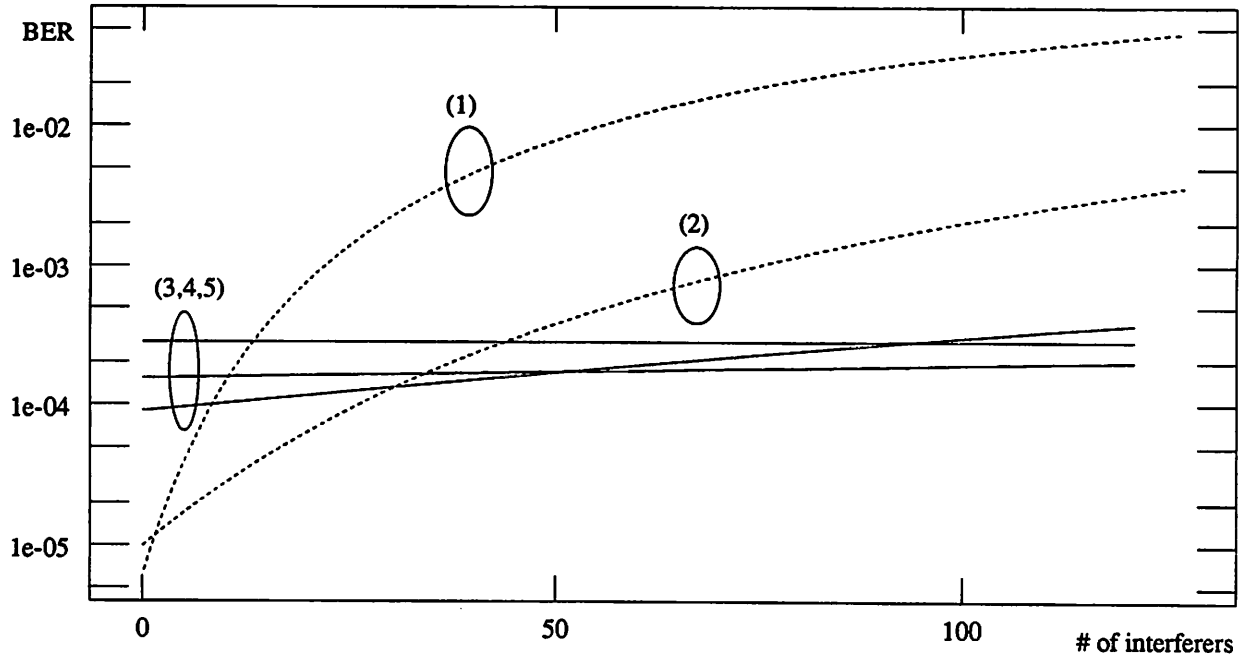


Fig. 13 BER versus the number of interferers ($m = 0, 1, \dots, 127$) in the downlink of a Rician fading channel for MRC (1), EGC (2), and CE for $TLR = -25.9$ dB (3), $TLR = -13.8$ dB (4), and $TLR = -9.0$ dB (5). The SNR is 10dB, $\bar{p}_0 = 0.1$, $K = 5$, and $N = 128$.

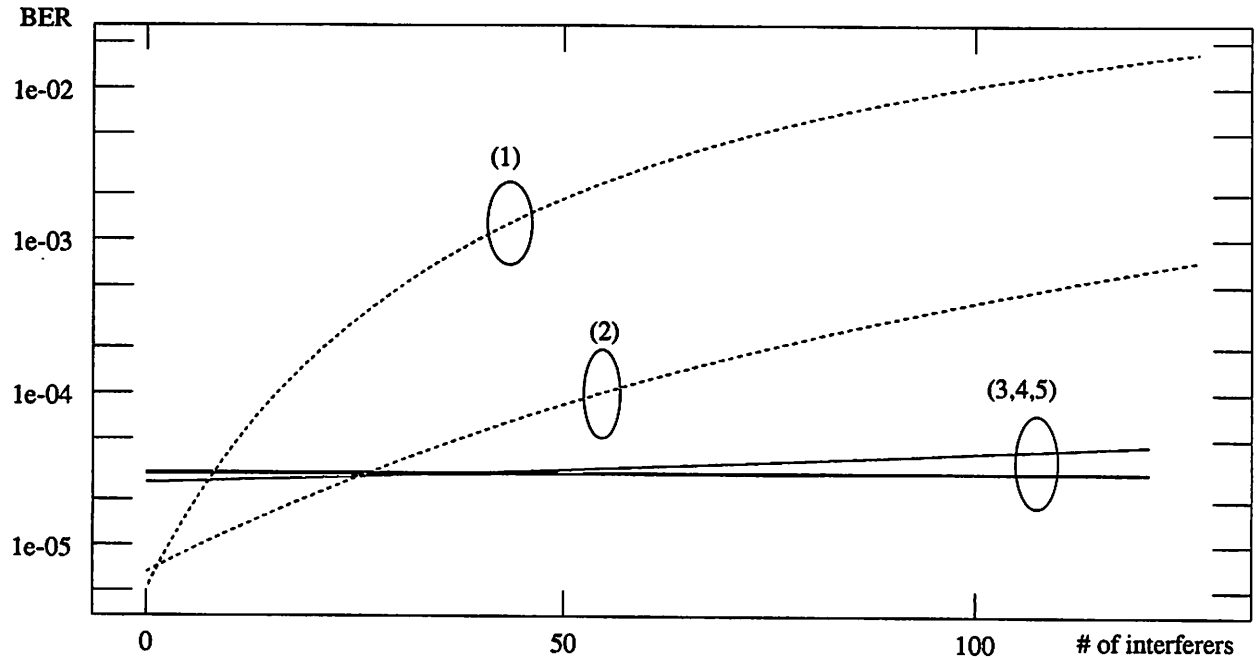


Fig. 14 BER versus the number of interferers ($m = 0, 1, \dots, 127$) in the downlink of a Rician fading channel for MRC (1), EGC (2), and CE for TLR = -7.8 dB (3), TLR = -25.9 dB (4), and TLR = -13.8 dB (5). The SNR is 10dB, $\bar{p}_0 = 0.1$, $K = 10$, and $N = 128$.

In this document, a novel digital modulation technique called Multi-Carrier Code Division Multiple Access was introduced and analyzed in both Rayleigh and Rician fading channels. The performance of this technique, gauged by the average bit error rate, was analytically and numerically evaluated for three equalization techniques that fall under classical diversity techniques. These techniques, Equal Gain Combining, Maximal Ratio Combining, and Controlled Equalization, perform equalization in the frequency domain, taking the component of each subcarrier (which represents the fading of the channel at a corresponding frequency) and performing a multiplicative operation on this component.

MC-CDMA appears to be a new promising spread spectrum-multiple access technique. It appears to be most effective in the downlink where phase control is most easily implemented. In the downlink, it was found that CE outperforms EGC and MRC in combating interference. It can also operate well in channels with large delay spreads: an assumption of independent fading at the subcarriers corresponds to a DS-SS system in which the number of resolvable paths is equal to the spreading factor. Since the F -parameter can be freely chosen, the spacing between subcarriers can be chosen so that MC-CDMA will exploit frequency diversity without excessive spreading factors.

In the uplink of a MC-CDMA communications system, it was found that because of the lack of phase control the codes and the orthogonality between users is invalidated. As the effectiveness of CE depends on restoring the orthogonality between users, it was not considered in the uplink. Thus, unless a remedy is applied to compensate for this deficiency, the coding of the subcarriers has no effect and consequently, the equalization techniques that were considered have no ability to combat the interference besides the redundancy in transmissions at multiple subcarriers. Thus, as one would expect, MRC, which is the optimal equalization in a noise-only channel, outperforms EGC. A possible solution to the phase distortion problem is predistortion in the transmitters. With this technique, each transmitter makes a measurement

of the channel and modifies the signal that it transmits so that at the receiving end, the signal that is obtained is the original signal that it intended to transmit.

For downlink transmissions, the following pattern was observed. For a very low number of users, MRC outperforms all equalization techniques. This result agrees with intuition since this corresponds to a noise-limited channel. For interference-limited channels, CE outperforms all techniques. This results because CE makes a direct attempt at combating interference. In between these two extremes, EGC performed the best for a "medium" load. While not distorting the orthogonality between users as with MRC and while not over amplifying the noise as with CE, EGC finds the balance between these extremes.

Thus, these equalization techniques have two conflicting goals: to combat noise and to combat interference. In the process of combating one form of degradation, the receiver becomes more susceptible to the other. EGC may be desirable for its simplicity, MRC in systems where a low number of users are expected, and CE for interference-limited channels. It should be noted that future communication systems tend to be headed in the direction of interference-limited channels, as they attempt to multiplex as many users as possible using the same resources.

While these techniques are not optimal in the sense that they do not address the minimization of some performance parameter, they are noteworthy for their relative simplicity and their intuitive feel for the underlying effects of the coding of the subcarriers. It should be noted that although CE is not optimal, it produces low BERs that are close to the theoretical minimum that are obtainable in a noise-only Rician fading channel (using MRC) with $K = 10$. A more formal (and more complicated) approach may be taken with multi-signal/multi-user detection to minimize the interference plus noise power in the decision process. With these schemes, each receiver considers the signals designated for all users simultaneously to decide what was transmitted from the desired user.

Appendix A: Statistical Properties of the Noise at the Input of the Slicer

0.1 EGC and MRC

The calculation of the statistical characterization of the noise at the input of the slicer for EGC and MRC are discussed together because of their mathematical similarities. As given in Eq. (17), the noise component is given as

$$\eta = \sum_{i=0}^{N-1} \int_{kT_b}^{(k+1)T_b} n(t) \frac{2}{T_b} d_{0,i} \cos(2\pi f_c t + 2\pi i \frac{F}{T_b} t + \theta_{0,i}) dt. \quad (\text{A-1})$$

Assuming that there are large number of subcarriers, i.e, N is large, the distribution of the η can be approximated by a Gaussian distribution by the Central Limit Theorem (CLT). The mean of η is given as

$$E\eta = \sum_{i=0}^{N-1} \int_{kT_b}^{(k+1)T_b} \overbrace{E n(t)}^0 \frac{2}{T_b} E d_{0,i} E \{ \cos(2\pi f_c t + 2\pi i \frac{F}{T_b} t + \theta_{0,i}) \} dt = 0. \quad (\text{A-2})$$

The variance of η can be determined as follows

$$\begin{aligned} \sigma_\eta^2 &= E\eta^2 \\ &= E \left\{ \left[\sum_{i=0}^{N-1} \int_{kT_b}^{(k+1)T_b} n(t_1) \frac{2}{T_b} d_{0,i} \cos(2\pi f_c t_1 + 2\pi i \frac{F}{T_b} t_1 + \theta_{0,i}) dt_1 \right] \times \right. \\ &\quad \left. \left[\sum_{j=0}^{N-1} \int_{kT_b}^{(k+1)T_b} n(t_2) \frac{2}{T_b} d_{0,j} \cos(2\pi f_c t_2 + 2\pi j \frac{F}{T_b} t_2 + \theta_{0,j}) dt_2 \right] \right\} \\ &= \sum_{i=0}^{N-1} \sum_{j=0}^{N-1} \int_{kT_b}^{(k+1)T_b} \int_{kT_b}^{(k+1)T_b} \frac{4}{T_b^2} E \{ n(t_1) n(t_2) \} E \{ d_{0,i} d_{0,j} \} \times \\ &\quad E \{ \cos(2\pi f_c t_1 + 2\pi i \frac{F}{T_b} t_1 + \theta_{0,i}) \cos(2\pi f_c t_2 + 2\pi j \frac{F}{T_b} t_2 + \theta_{0,j}) \} dt_1 dt_2 \\ &= \sum_{i=0}^{N-1} \sum_{j=0}^{N-1} \int_{kT_b}^{(k+1)T_b} \int_{kT_b}^{(k+1)T_b} \frac{4}{T_b^2} \frac{N_0}{2} \delta(t_1 - t_2) E \{ d_{0,i} d_{0,j} \} \times \\ &\quad E \{ \cos(2\pi f_c t_1 + 2\pi i \frac{F}{T_b} t_1 + \theta_{0,i}) \cos(2\pi f_c t_2 + 2\pi j \frac{F}{T_b} t_2 + \theta_{0,j}) \} dt_1 dt_2 \\ &= \sum_{i=0}^{N-1} \sum_{j=0}^{N-1} \int_{kT_b}^{(k+1)T_b} \frac{2}{T_b^2} N_0 E \{ d_{0,i} d_{0,j} \} \times \\ &\quad E \{ \cos(2\pi f_c t_1 + 2\pi i \frac{F}{T_b} t_1 + \theta_{0,i}) \cos(2\pi f_c t_1 + 2\pi j \frac{F}{T_b} t_1 + \theta_{0,j}) \} dt_1 \end{aligned}$$

$$\begin{aligned}
 &= \sum_{i=0}^{N-1} \sum_{j=0}^{N-1} \frac{2}{T_b} N_0 E \{d_{0,i} d_{0,j}\} \times \\
 &E \int_{kT_b}^{(k+1)T_b} \left[\frac{1}{2} \cos \left(2\pi F \frac{i-j}{T_b} t_1 + \theta_{0,i} - \theta_{0,j} \right) + \frac{1}{2} \cos \left(4\pi f_c t_1 + 2\pi F \frac{i+j}{T_b} t_1 + \theta_{0,i} + \theta_{0,j} \right) \right] dt_1 \\
 &\cong \sum_{i=0}^{N-1} \sum_{j=0}^{N-1} \frac{2}{T_b} N_0 E \{d_{0,i} d_{0,j}\} E \int_{kT_b}^{(k+1)T_b} \frac{1}{2} \cos \left(2\pi F \frac{i-j}{T_b} t_1 + \theta_{0,i} - \theta_{0,j} \right) dt_1 \\
 &= \sum_{i=0}^{N-1} \frac{2}{T_b} N_0 E d_{0,i}^2 \frac{1}{2} T_b = N \frac{N_0}{T_b} E d_{0,i}^2 \tag{A-3}
 \end{aligned}$$

where the following approximation and identity were used

$$\int_{kT_b}^{(k+1)T_b} \cos \left(4\pi f_c t_1 + 2\pi F \frac{i+j}{T_b} t_1 + \theta_{0,i} + \theta_{0,j} \right) dt_1 \cong 0 \tag{A-4}$$

$$\sum_{i=0}^{N-1} \sum_{j=0}^{N-1} \int_{kT_b}^{(k+1)T_b} \frac{1}{2} \cos \left(2\pi F \frac{i-j}{T_b} t_1 + \theta_{0,i} - \theta_{0,j} \right) dt_1 = 0. \tag{A-5}$$

The approximation of Eq. (A-4) holds if $\frac{2f_c + F(i+j)}{T_b} \gg \frac{1}{T_b}$. This condition is satisfied with the carrier frequency (in the GHz range) and symbol rates (on the order of Mbauds/sec) of interest. Eq. (A-5) results from the integral over an integer number of the period of a cosine wave with period $T_b/[F(i-j)]$ for $i \neq j$.

0.1.1 EGC

For EGC in a Rayleigh or Rician fading channel, the variance of the noise is given as

$$\sigma_{\eta}^2 = N \frac{N_0}{T_b}. \tag{A-6}$$

0.1.2 MRC

For MRC in a Rayleigh or Rician fading channel, the variance of the noise is given as

$$\sigma_{\eta}^2 = N \frac{N_0}{T_b} E \rho_{0,i}^2 = 2 \frac{N_0}{T_b} P_0. \tag{A-7}$$

0.2 CE

The derivation of the distribution of the noise for CE is similar to that of EGC and MRC. Given that there are n_0 subcarriers above the threshold indexed by j , the noise component in the decision variable is

$$\eta = \sum_j d_{0,j} \int_{iT_b}^{(k+1)T_b} n(t) \frac{2}{T_b} \cos(2\pi f_c t + 2\pi j \frac{F}{T_b} t + \theta_{0,j}) dt = \sum_j \eta_{0,j} d_{0,j}. \quad (\text{A-8})$$

As the noise term is the sum of n_0 independent random variables (r.v.), where n_0 will be large with a high probability for the values of ρ_{thresh} of interest, the noise can be approximated by the CLT to be a zero-mean Gaussian r.v. with a variance given in Eq. (A-3) as

$$\sigma_{\eta|n_0}^2 = n_0 \frac{N_0}{T_b} E d_{0,j}^2 \quad (\text{A-9})$$

where N has been replaced by n_0 . For a Rayleigh fading channel, i.e., $\rho_{0,i}$ is Rayleigh distributed, the variance of the noise is given as

$$\sigma_{\eta|n_0}^2 = n_0 \frac{N_0}{T_b} \frac{1}{2\rho_{0,i}} \frac{1}{pr_{on}} E_1\left(\frac{\rho_{thresh}^2}{2\rho_{0,i}}\right) \quad (\text{A-10})$$

where $\overline{\rho_{0,i}}$ is the local-mean power of the i th subcarrier, $E_1(\rho)$ is the exponential integral defined as [17]

$$E_1(\rho) = \int_{\rho}^{\infty} \frac{e^{-t}}{t} dt = -\gamma - \ln(\rho) - \sum_{n=1}^{\infty} \frac{(-1)^n \rho^n}{n(n!)} \quad (\text{A-11})$$

with $\gamma = 0.5772157$, and the probability that a subcarrier is above the threshold, pr_{on} , for Rayleigh fading is given as

$$pr_{on} = \int_{\rho_{thresh}}^{\infty} \frac{\rho}{P_{0,i}} e^{-\frac{\rho^2}{2P_{0,i}}} d\rho = e^{-\frac{\rho_{thresh}^2}{2P_{0,i}}}. \quad (\text{A-12})$$

For Rician fading, the variance of the noise is given as

$$\sigma_{\eta|n_0}^2 = n_0 \frac{N_0}{T_b} \frac{1}{2\rho_{0,i}} \frac{1}{pr_{on}} \int_{\rho_{thresh}}^{\infty} (K+1) e^{-K} \frac{1}{\rho_{0,i} P_{0,i}} e^{-\frac{K+1}{2\rho_{0,i}} \rho_{0,i}^2} I_0\left(\rho_{0,i} \sqrt{\frac{2K(K+1)}{P_{0,i}}}\right) d\rho_{0,i} \quad (\text{A-13})$$

where

$$pr_{on} = \int_{\rho_{thresh}}^{\infty} (K+1) e^{-K} \frac{\rho_{0,i}}{P_{0,i}} e^{-\frac{K+1}{2\rho_{0,i}} \rho_{0,i}^2} I_0\left(\rho_{0,i} \sqrt{\frac{2K(K+1)}{P_{0,i}}}\right) d\rho_{0,i}. \quad (\text{A-14})$$

Appendix B: Statistical Properties of the Interference (at the Input to the Slicer)

The following statistical identities will be used

$$Ea_m[k] = \frac{1}{2}(-1) + \frac{1}{2}(1) = 0 \quad Ea_m^2[k] = \frac{1}{2}(-1)^2 + \frac{1}{2}(1)^2 = 1$$

$$E\cos^2(\theta_{0,i} - \theta_{m,i}) = \int_0^{2\pi} \frac{1}{2\pi} \cos^2 \tilde{\theta}_{m,i} d\tilde{\theta}_{m,i} = \frac{1}{2} \quad (B-1)$$

0.1 Uplink

0.1.1 EGC

The interference component, β_{int} , for EGC is given as

$$\beta_{int} = \sum_{m=1}^{M-1} a_m[k] \sum_{i=0}^{N-1} c_m[i] c_0[i] \rho_{m,i} \cos \tilde{\theta}_{m,i} \quad (B-2)$$

Since the in-phase component of a Rayleigh random variable, $\rho_{m,i} \cos \tilde{\theta}_{m,i}$, is Gaussian and $a_m[k] c_m[i] c_0[i] \in \{-1, 1\}$, β_{int} consists of the sum of $(M-1) \times N$ iid Gaussian r.v.'s. Thus, β_{int} is Gaussian with a mean of

$$E\beta_{int} = \sum_{m=1}^{M-1} \sum_{i=0}^{N-1} E\{a_m[k] \rho_{m,i} c_m[i] c_0[i] \cos \tilde{\theta}_{m,i}\}$$

$$= \sum_{m=1}^{M-1} E a_m[k] \sum_{i=0}^{N-1} c_m[i] c_0[i] E \rho_{m,i} E \cos \tilde{\theta}_{m,i} = 0 \quad (B-3)$$

and a variance of

$$\sigma_{\beta_{int}}^2 = (M-1) N E \{a_m[k] \rho_{m,i} c_m[i] c_0[i] \cos \tilde{\theta}_{m,i}\}^2$$

$$= (M-1) N c_m^2[i] c_0^2[i] E a_m^2[k] E \rho_{m,i}^2 E \cos^2 \tilde{\theta}_{m,i}$$

$$= \frac{1}{2} (M-1) N E \rho_{m,i}^2 = (M-1) \overline{p_m} \quad (B-4)$$

If $\rho_{0,i}$ has a Rician distribution, then the interference can be approximated by the CLT as a Gaussian r.v. since it consists of a sum of iid r.v.'s. Thus, β_{int} will have the same mean and variance expression as in Eq. (B-3) and Eq. (B-4). Note that this is true for the variance of the interference since the local-mean power for Rayleigh and Rician fading are defined by the same quantity

$$\overline{p_{m,i}} = \frac{1}{2} E \rho_{m,i}^2.$$

0.1.2 MRC

For MRC, the interference component is given as

$$\beta_{int} = \sum_{m=1}^{M-1} a_m[k] \sum_{i=0}^{N-1} c_m[i] c_0[i] \rho_{m,i} \rho_{0,i} \cos \tilde{\theta}_{m,i} \quad (\text{B-5})$$

As β_{int} is composed of $(M-1) \times N$ iid r.v.'s, it can be approximated by a Gaussian distribution using the CLT for both Rayleigh and Rician fading with a mean of

$$\begin{aligned} E\beta_{int} &= (M-1)NE \{a_m[k] \rho_{m,i} c_m[i] c_0[i] \cos \tilde{\theta}_{m,i}\} \\ &= (M-1)NE \{a_m[k]\} c_m[i] c_0[i] E\rho_{m,i} E\rho_{0,i} E\cos \tilde{\theta}_{m,i} = 0 \end{aligned} \quad (\text{B-6})$$

and a variance of

$$\begin{aligned} \sigma_{\beta_{int}}^2 &= (M-1)NE \{a_m[k] \rho_{m,i} \rho_{0,i} c_m[i] c_0[i] \cos(\theta_{0,i} - \theta_{m,i})\}^2 \\ &= (M-1)Nc_m^2[i] c_0^2[i] Ea_m^2[k] E\rho_{m,i}^2 E\rho_{0,i}^2 E\cos^2(\theta_{0,i} - \theta_{m,i}) \\ &= \frac{1}{2} (M-1)NE\rho_{m,i}^2 E\rho_{0,i}^2 = 2 \frac{(M-1)}{N} \overline{p_m p_0}. \end{aligned} \quad (\text{B-7})$$

0.2 Downlink

0.2.1 EGC

For downlink transmissions using EGC, the interference component is

$$\beta_{int} = \sum_{m=1}^{M-1} a_m[k] \left(\sum_{j=0}^{\frac{N}{2}-1} \rho_{0,a_j} - \sum_{j=0}^{\frac{N}{2}-1} \rho_{0,b_j} \right) \quad (\text{B-8})$$

Applying the CLT independently to both inner summations yields two identical Gaussian random variables. Thus, β_{int} may be approximated by a zero-mean Gaussian r.v. with a variance of

$$\begin{aligned} \sigma_{\beta_{int}}^3 &= (M-1)N\sigma_{\rho_{0,i}}^2 = (M-1)N(E\rho_{0,i}^2 - E^2\rho_{0,i}) = (M-1)N(2\overline{p_{0,i}} - \frac{\pi}{2}\overline{p_{0,i}}) \\ &= 2(M-1)(1 - \frac{\pi}{4})\overline{p_0} \end{aligned} \quad (\text{B-9})$$

for Rayleigh fading and

$$\sigma_{\beta_{int}}^3 = (M-1)N\sigma_{\rho_{0,i}}^2 = 2(M-1)(1-\gamma)\overline{p_0} \quad (\text{B-10})$$

for Rician fading, where

$$\gamma = \frac{\pi}{4} \left(\frac{e^{-K}}{K+1} \right) \left[(1+K) I_0 \left(\frac{K}{2} \right) + K I_1 \left(\frac{K}{2} \right) \right]^2. \quad (\text{B-11})$$

0.2.2 MRC

For MRC in the downlink, the decision variable is given as

$$\beta_{int} = \sum_{m=1}^{M-1} a_m [k] \left(\sum_{j=0}^{\frac{N}{2}-1} \rho_{0,a_j}^2 - \sum_{j=0}^{\frac{N}{2}-1} \rho_{0,b_j}^2 \right). \quad (\text{B-12})$$

Applying the CLT in the same manner as with EGC, the interference can be approximated by a zero-mean Gaussian r.v. with a variance of

$$\sigma_{\beta_{int}}^2 = (M-1)N [E\rho_{0,i}^4 - (E\rho_{0,i}^2)^2] = (M-1)N (8\overline{p_{0,i}^2} - 4\overline{p_{0,i}}^2) = \left(\frac{M-1}{N} \right) 4\overline{p_0}^2 \quad (\text{B-13})$$

for Rayleigh fading and

$$\sigma_{\beta_{int}}^2 = (M-1)N [E\rho_{0,i}^4 - (E\rho_{0,i}^2)^2] = \left(\frac{M-1}{N} \right) \frac{8K+4}{(K+1)^2} \overline{p_0}^2 \quad (\text{B-14})$$

for Rician fading.

Appendix C: Simplification of CLT Expressions

Assume the conditional BER to have the following general form

$$pr(error|\rho) = \frac{1}{2} \operatorname{erfc} \left(\sqrt{\frac{\frac{1}{2}\rho}{\sigma_{\beta_{ini}}^2 + \sigma_{\eta}^2}} \right) = \int_{\rho}^{\infty} \frac{1}{\sqrt{2\pi(\sigma_{\beta_{ini}}^2 + \sigma_{\eta}^2)}} e^{-\frac{y^2}{2(\sigma_{\beta_{ini}}^2 + \sigma_{\eta}^2)}} dy. \quad (\text{C-1})$$

Assuming that ρ has a Gaussian distribution with mean μ and variance σ^2 , the average BER can be simplified as follows

$$\begin{aligned} BER &= \int_{-\infty}^{\infty} \frac{1}{\sqrt{2\pi\sigma^2}} e^{-\frac{(\rho-\mu)^2}{2\sigma^2}} \int_{\rho}^{\infty} \frac{1}{\sqrt{2\pi(\sigma_{\beta_{ini}}^2 + \sigma_{\eta}^2)}} e^{-\frac{y^2}{2(\sigma_{\beta_{ini}}^2 + \sigma_{\eta}^2)}} dy d\rho \quad (\text{C-2}) \\ &= \int_0^{\infty} \frac{1}{\sqrt{(2\pi)^2 \sigma^2 (\sigma_{\beta_{ini}}^2 + \sigma_{\eta}^2)}} \int_{-\infty}^{\infty} e^{-\frac{(\rho-\mu)^2}{2\sigma^2} - \frac{(x+\rho)^2}{2(\sigma_{\beta_{ini}}^2 + \sigma_{\eta}^2)}} d\rho dx \\ &= \int_0^{\infty} \frac{1}{\sqrt{(2\pi)^2 \sigma^2 (\sigma_{\beta_{ini}}^2 + \sigma_{\eta}^2)}} e^{-\frac{1}{2\sigma^2(\sigma_{\beta_{ini}}^2 + \sigma_{\eta}^2)} \left[\frac{\{\mu(\sigma_{\beta_{ini}}^2 + \sigma_{\eta}^2) - x\sigma^2\}^2}{\sigma_{\beta_{ini}}^2 + \sigma_{\eta}^2 + \sigma^2} + \mu^2(\sigma_{\beta_{ini}}^2 + \sigma_{\eta}^2) + x^2\sigma^2 \right]} dx \\ &\quad \times \int_{-\infty}^{\infty} e^{-\frac{1}{2\sigma^2(\sigma_{\beta_{ini}}^2 + \sigma_{\eta}^2)} \left[\sqrt{\sigma_{\beta_{ini}}^2 + \sigma_{\eta}^2 + \sigma^2} \rho - \frac{\mu(\sigma_{\beta_{ini}}^2 + \sigma_{\eta}^2) - x\sigma^2}{\sqrt{\sigma_{\beta_{ini}}^2 + \sigma_{\eta}^2 + \sigma^2}} \right]^2} d\rho dx \\ &= \int_0^{\infty} \frac{1}{\sqrt{2\pi(\sigma_{\beta_{ini}}^2 + \sigma_{\eta}^2 + \sigma^2)}} e^{-\frac{1}{2\sigma^2(\sigma_{\beta_{ini}}^2 + \sigma_{\eta}^2)} \left[\frac{\{\mu(\sigma_{\beta_{ini}}^2 + \sigma_{\eta}^2) - x\sigma^2\}^2}{\sigma_{\beta_{ini}}^2 + \sigma_{\eta}^2 + \sigma^2} + \mu^2(\sigma_{\beta_{ini}}^2 + \sigma_{\eta}^2) + x^2\sigma^2 \right]} dx \\ &= \frac{1}{\sqrt{2\pi(\sigma_{\beta_{ini}}^2 + \sigma_{\eta}^2 + \sigma^2)}} \int_0^{\infty} e^{-\frac{1}{2(\sigma_{\beta_{ini}}^2 + \sigma_{\eta}^2 + \sigma^2)} \frac{(x+\mu)^2}{\sigma^2}} dx \\ &= \frac{1}{\sqrt{\pi}} \int_{\mu}^{\infty} e^{-t^2} dt \\ &\quad \frac{1}{\sqrt{2(\sigma_{\beta_{ini}}^2 + \sigma_{\eta}^2 + \sigma^2)}} \\ &= \frac{1}{2} \operatorname{erfc} \left(\sqrt{\frac{\frac{1}{2}\mu}{\sigma^2 + \sigma_{\beta_{ini}}^2 + \sigma_{\eta}^2}} \right). \quad (\text{C-3}) \end{aligned}$$

References

- [1] N. Yee, J. P. Linnartz and G. Fettweis, "Multi-Carrier CDMA in Indoor Wireless Radio Networks," Proceedings PIMRC '93, Yokohama, Japan, 1993, pp. 109-113.
- [2] G. Fettweis, "Multi-Carrier Code Division Multiple Access (MC-CDMA): Basic Idea," Technikon Communication Systems - Internal Report.
- [3] K. Fazel and L. Papke, "On the Performance of Convolutionally - Coded CDMA/OFDM for Mobile Communication System," Proceedings PIMRC '93, Yokohama, Japan, 1993, pp. 468-472.
- [4] Leonard J. Cimini, Jr., "Analysis and Simulation of a Digital Mobile Channel Using Orthogonal Frequency Division Multiplexing," *IEEE Transactions on Communications*, vol. COM-33, pp. 665-6.
- [5] Michel Alard and Roselyne Lassalle, "Principles of Modulation and Channel Coding for Digital Broadcasting for Mobile Receivers," *EBU Review - Technical*, no. 224, pp. 168-190, 1987.
- [6] J. Proakis, *Digital Communications*, New York: McGraw-Hill, 1983, Ch. 4.
- [7] R. Ganesh and K. Pahlavan, "Effects of Traffic and Local Movements on Multipath Characteristics of an Indoor Radio Channel," *Electronics Letters*, vol. 26, no. 12, June 1990, pp. 810-12.
- [8] S. Howard and K. Pahlavan, "Doppler Spread Measurements of the Indoor Radio Channel," *Electronic Letters*, v. 26, no. 2, 1990, pp. 107-109.
- [9] Robert Bultitude, "Measurement, Characterization and Modelling of Indoor 800/900 MHz Radio Channels for Digital Communications," *IEEE Communications Magazine*, v. 25, no. 6, pp. 5-12, June 1987.
- [10] R. Bultitude, S. Mahmoud and W. Sullivan, "A Comparison of Indoor Radio Propagation Characteristics at 910 MHz and 1.75 GHz," *IEEE Journal on Selected Areas in Communications*, vol. 7, no. 1, Jan. 1989, pp. 20-30.
- [11] Adel A.M. Saleh and Reinaldo A. Venueza, "A Statistical Model for Indoor Multipath Propagation," *IEEE Journal on Selected Areas in Communications*, vol. SAC-5, no. 2, pp. 128-137, Feb. 1987.
- [12] Thomas A. Sexton and Kaveh Pahlavan, "Channel Modeling and Adaptive Equalization of Indoor Radio Channels," *IEEE Journal on Selected Areas in Communications*, vol. 7, no. 1, pp. 114-120, Jan. 1989.
- [13] J. P. Linnartz, *Narrowband Land-Mobile Networks*, Artech House, Norwood MA, 1993.
- [14] R. L. Pickholtz, D. L. Schilling and L.B. Milstein, "Theory of Spread-Spectrum Communications - A Tutorial," *IEEE Transactions on Communications*, COM-30, May 1982, pp.855-884.
- [15] Rodger E. Zeimer and Roger L. Peterson, *Digital communications and spread spectrum systems*, New York: Macmillan; London: Collier Macmillan, c1985.
- [16] N. C. Beaulieu, "Infinite Series for the Computation of the Complementary Probability Distribution Function as a Sum of Independent Random Variables and Its Application to the Sum of Rayleigh Random Variables," *IEEE Transactions on Communications*, vol. 38, no. 9, Sept. 1990, pp. 1463-1474.
- [17] M. Abramowitz and L. A. Stegun, *Handbook of Mathematical Functions: with Formulas, Graphs, and Mathematical Tables*, New York: Dover Publications, 1970.